# The 16<sup>th</sup> Symposium on Polar Science

2-5 December 2025

# National Institute of Polar Research Research Organization of Information and Systems

Session OG

Polar Geosciences

# Abstracts

Conveners: Yusuke Suganuma, and Kenji Horie (NIPR)

### **Development Status of the Separation Mechanism for Stable Penetration of Penetrators**

Kodai Yamamoto<sup>1</sup>, Masa-yuki Yamamoto<sup>1</sup>, Yasuhiro Nishikawa<sup>1,2</sup>, Kazuto Saiki<sup>3</sup>, Ryota Taniguchi<sup>3</sup>, Takamasa Hiratsuka<sup>1</sup>, Naoyuki Kurita<sup>4</sup> and Satoshi Tanaka<sup>5</sup>

<sup>1</sup>Kochi University of Technology

<sup>2</sup>Osaka Kyoiku University

<sup>3</sup>Ristumeikan University

<sup>4</sup>Nagoya University

<sup>5</sup> Insitute of Space and Astronautical Science (ISAS), JAXA

The AH1002 penetrator group deployed three penetrators onto the Shirase Glacier at JARE66 (Japanese Antarctic Research and Expedition 66th). One of the penetrators has been confirmed operation for over six months, transmitting positional information and environmental data from January to August. However, communication with the other two penetrators was lost after penetration. The cause was thought to be communication failure due to issues with post-penetration orientation or penetration depth. Based on these results, we analysed the necessary elements for future penetrator development by refocusing on the penetration operation. When used in typical Japanese soil, the penetration status typically follows a half-penetration or full-penetration pattern. according to JARE43 Matsushima et. al., and JARE64 Nishikawa et al., the penetrator's penetration behaviour is known to result in over-penetration. <sup>1,2)</sup> For JARE66, measures such as reducing weight were implemented to stabilise penetration depth and attitude, with the result that communication was lost. To support diverse penetration status, it was found necessary to install the Antarctic penetrator with a separation mechanism. Historically, the afterbody configuration was a proposed structural approach for penetrator separation mechanisms. Investigation of past penetrator designs revealed the aft-body configuration. This structure was originally developed for NASA's Mars Polar Lander<sup>3)</sup>. The idea of the afterbody structure is to stabilise the function of each component by separating them: placing observation instruments on the subsurface side and communication equipment on the ground surface side. We examined the afterbody structure concept and designed and developed a separation mechanism. The mechanism's operation utilises the impact force experienced by the penetrator during penetration to fracture the bolts securing the joint (bolt-separated mechanism) (Figure 1a). In order to investigate the bolt separated operation, drop tests were conducted at Kyoto-Miyazu (lunar environment) and Antarctic ice sheet-S16 (Figure 2). The penetration sutatus confirmed the mechanism of bolt-separating mechanism during semi-penetration and over-penetration, demonstrating the separation method via bolt fracture as viable. However, it was also found that the aft-body part remained unexposed during over-penetration. To address this issue, a tail-lifting mechanism was designed, incorporating spring release, cable connection, and a combination of these mechanisms (Figure 1b). The advantage of the tail-lifting mechanism, developed and studied in the DS-2 and Ice Penetrator<sup>4</sup>), is that separation is achieved by bolt shear failure utilising the penetration impact force and the inertial force of the aft-body section, rather than the tail section absorbing the impact. This failure mechanism provides a degree of active control through spring elastic force, compared to preventing over-penetration by enlarging the tail diameter. Disadvantages include the need to evaluate the strength and length of the connecting wire for the tail section. Additionally, determining the required spring constant for the flipping action and ensuring the electrical system cables are adequately secured are further considerations. Implementing the tail-lifting mechanism enables enhancements such as post-penetration communication stability and the addition of solar panels for long-term observation, promising further robust enhancement of the penetrator. Operational testing of these mechanisms is scheduled for verification at the Kochi Prefecture test field (planned for mid-September to October). Furthermore, verification of reproducing the overpenetration state is planned for Niigata Prefecture (scheduled for December to January).

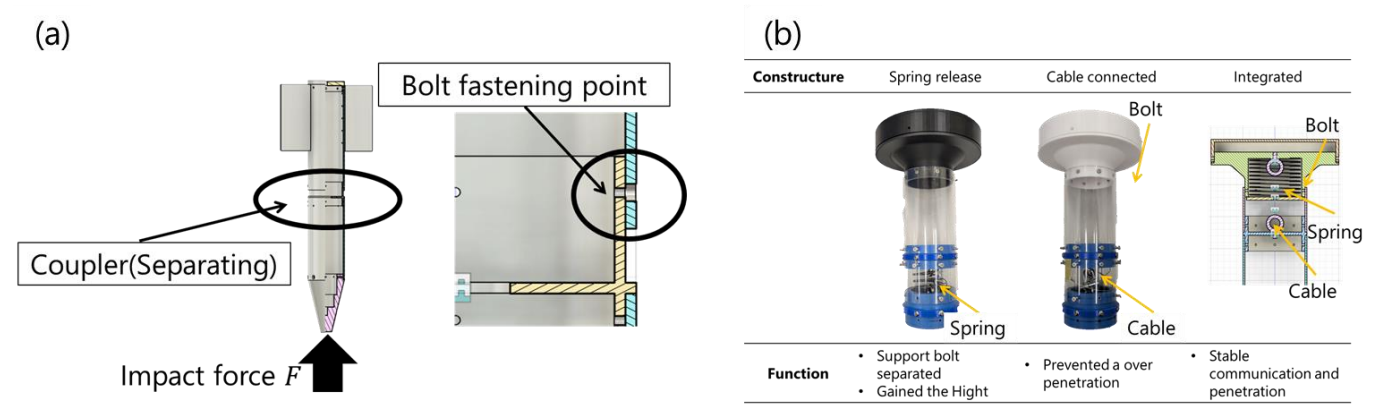


Figure 1. Bolt separation mechanics(a) and another mechanims(b) for stable penetration and communication.



Figure 2. Deployment tests utilising bolt separation were conducted in lunar (a) and icy satellite (b) environments.

#### References

- 1) Matsushima, T., Yamashita, M., Yasuhara, T., Horiguchi, K., Miyamachi, H., Toda, S., Takada, M., Watanabe, A., & Shibuya, K. (2003). Observation tests of the Antarctic penetrator on the Mizuho Plateau in JARE-43 summer operation. *Antarctic Record*, **47**(3), 395–408.
- 2) Nishikawa, Y., Yamamoto, K., & Tanaka, S. (2024). A report on Penetrators for Antarctic on the 64th Japanese Antarctic Research Expedition. *Antarctic Record*, **68**, 1–20.
- 3) Smrekar, S. E., Catling, D. C., Lorenz, R. D., Magalhães, J. A., Moersch, J. E., Morgan, P., and Blaney, D. L. (1999). Deep Space 2: The Mars microprobe mission. *J. Geophysical Research: Planets*, **104**(E11), 27013–27030.
- 4) Brown, M. J. (2023). Mechanical shock analysis and testing of an air-dropped Antarctic ice penetrator (Master's thesis, Massachusetts Institute of Technology). DSpace@MIT.

### Experimental Validation of an Antarctic Observation Penetrator at the Shirase Glacier

<u>Kazuto SAIKI<sup>1</sup></u>, Gaku HAMAJIMA<sup>2</sup>, Ryota TANIGUCHI<sup>1</sup>, Satoshi TANAKA<sup>3</sup>, Yasuhiro NISHIKAWA<sup>2,4</sup>, Kodai YAMAMOTO<sup>2</sup>, and Takamasa HIRATSUKA<sup>2</sup>

<sup>1</sup>Ritsumeikan Univsersity
<sup>2</sup>Kochi University of Technology
<sup>3</sup>Institute of Space and Astronautical Science (ISAS), JAXA
<sup>4</sup>Osaka Kyoiku Univsersity

The "penetrator" is a drop-and-embed observation system designed for deployment in locations where installation by humans is difficult or impossible due to distance or safety constraints. By releasing it from the air, the system embeds itself into the ground and enables the acquisition of seismic and/or other geophysical data through onboard instruments. During the 64th and 65th Japanese Antarctic Research Expeditions, preliminary experiments were conducted to verify the feasibility of the penetrator (1,2). In the 66th expedition, we carried out its first actual deployment from a manned helicopter into the Shirase Glacier, successfully establishing a long-term monitoring system for glacier flow.

### (1) Specifications and Objectives of the Penetrator

A demonstration experiment was conducted to deploy the drop-and-embed observation system, the penetrator, from a manned helicopter. The penetrator was equipped with a GPS receiver, thermometer, barometer, and accelerometer, and was installed on the Shirase Glacier with the aim of monitoring glacier flow and transmitting telemetry data to Japan via Iridium communication.

### (2) Deployment Training

At Kitanoura, training was conducted to accurately deploy the penetrator from a manned helicopter onto a designated latitude—longitude target. The target precision was set at within 100 m of the designated point, with deployment initiated once the helicopter reached coordinates within that range. Navigation based on latitude and longitude was handled by Taniguchi, assistance in transferring the penetrator and recording altitude was managed by Hamajima, and penetrator release was executed by Saiki.

On 29 December 2024, the team accessed the sea ice at Kitanoura via snowmobile and marked the intended target site for penetrator deployment using ice paint (Fig. 1). The latitude and longitude were recorded with a handheld GPS. On 30 December 2024, four penetrators were deployed from the helicopter. Although the original plan was to release them from an altitude of 400 m, overcast skies in the morning prevented flight operations. In the afternoon, flight was permitted below cloud level, and the deployment was conducted from an altitude of 300 m. A photograph of the penetrator release in progress is shown in Fig. 2. The designated target point was 69° 00′ 06.12″ S, 39° 35′ 59.41″ E.

On 31 December 2024, the penetrators were recovered using a snowmobile, though one (#2) of the four units could not be located. The penetration points were all within 100 m of the target. While this met the accuracy goal, the deviations from the helicopter's coordinates at the time of release were even smaller: 50 m for #1, 17 m for #3, and 26 m for #4. This indicates that navigation training could further improve precision. Because the ice was softer than in previous years, the penetrators penetrated more deeply, resulting in the loss of one unit.



Figure 1. Marking of the target site.



Figure 2. Deployment of penetrators from the helicopter.
Photo by N. Kitamoto (JARE66)



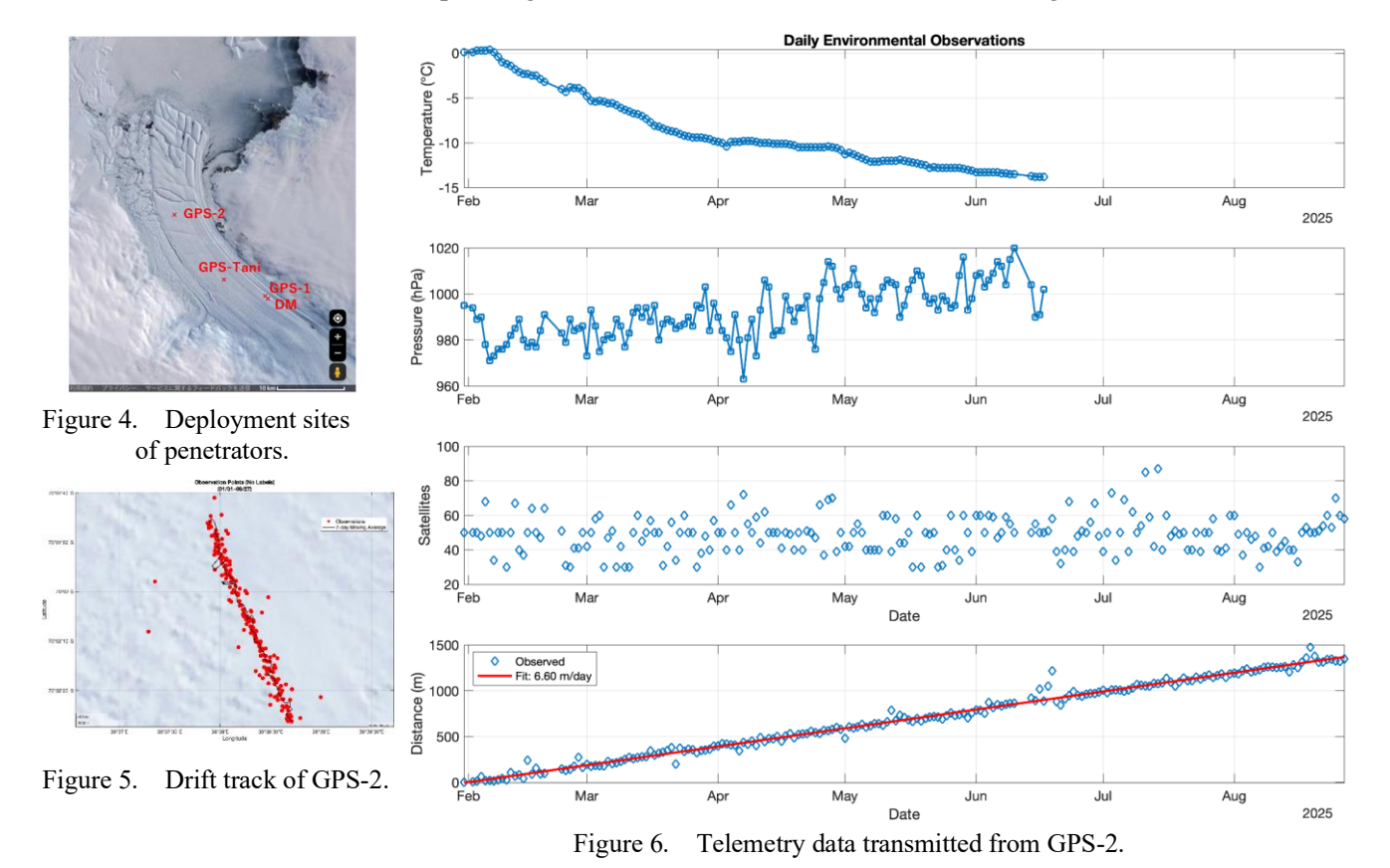
Figure 3. Deployment of a penetrator onto Shirase Glacier.

#### (3) Demonstration Test at the Shirase Glacier

On January 21, 2025, four penetrators were deployed from an AS helicopter onto the Shirase Glacier. The first was a dummy unit (DM) without onboard instruments, dropped from an altitude of 400 m to assess penetration depth, given concerns that the ice might be softer than in previous years. Subsequently, three GPS-equipped penetrators (GPS-1, GPS-Tani, and GPS-2) were deployed to the upper, middle, and lower reaches of the glacier (Fig.3), respectively, from altitudes of 400 m, 300 m, and 300 m. The deployment sites are shown in Fig. 4. After releasing the DM, the helicopter descended to check penetration. Since the tail section remained exposed above the surface, the ice was judged to be harder than at Kitanoura, and GPS-1 was also dropped from 400 m. GPS-1 likewise remained partially exposed. The GPS-Tani penetrator, which has a forward-shifted center of gravity and larger tail fins, was expected to achieve straighter and deeper penetration and was therefore deployed from 300 m. However, the impact site could not be located, suggesting it had penetrated too deeply. GPS-2, also dropped from 300 m, similarly could not be located and appeared to have penetrated deeply into the ice.

Back at Syowa Station, telemetry transmissions expected once per day were monitored. Telemetry was received from GPS-1, which had a partially exposed tail, but not from the other two units. GPS-1 also ceased transmission the following day. Although these results initially suggested failure, telemetry unexpectedly began to arrive from GPS-2 on January 31, followed by GPS positioning data from February 1 onward. While temperature and pressure data have not been received since June 18, GPS-2 has continued to transmit positioning data up to the time of writing (Fig. 5,6). Because the number of tracked satellites varied, deviations from the true positions are expected to fluctuate. Regarding the loss of contact with GPS-1, since the penetrator was visually confirmed after emplacement, it is presumed that the unit was not firmly fixed after penetration and was displaced by wind or other factors, resulting in an orientation that prevented communication. By contrast, the sudden recovery of GPS-2 is hypothesized to result from lower ambient temperatures, which froze small amounts of intergranular water in the ice, reducing radio wave attenuation.

The data transmitted from GPS-2, combined with glaciological observations from the AJ1004 team, are expected to contribute to quantitative evaluations of large-scale glacier retreat and glacier–ice shelf discharge mechanisms, which have become pressing issues in the context of recent climate change.



#### References

- 1) Nishikawa et al., An introduction to the penetrators for Antarctic regions, *The 14th Symposium on Polar Science*, 2023.
- 2) Tanaka et al., Drop and Installation Tests of Antarctic Penetrators Using a Drone and a Helicopter with Operational Seismic and Infrasound Observations, *The 15th Symposium on Polar Science*, 2024.

# Interactions of crustal and mantle materials in supracratonic metamorphic hard rock formations in the environment at the base of natural, great earthquake seismogenic zones

Hiroshi Ogasawara<sup>1</sup>, Yasuo Yabe<sup>2</sup>, and the ICDP DSeis/PROTEA team<sup>3,4,5</sup>

<sup>1</sup> Ritsumeikan University, <sup>2</sup> Tohoku University,

<sup>3</sup> https://www.ritsumei.ac.jp/~ogasawar/DSeis/TheDSeisTeam20230708.pdf,

<sup>4</sup> https://www.icdp-online.org/projects/by-continent/africa/dseis-south-africa/,

<sup>5</sup> https://www.icdp-online.org/projects/by-continent/africa/protea-south-africa/

This is a follow-up to the reports by Ogasawara et al. and Yabe et al. (OGo 13 and 14, respectively, at the 15th symposium in 2024). We report on the progress in 2025 in comparing the outcomes of ICDP drilling to probe the aftershock- and main-rupturezones of an M5.5 earthquake (DSeis/PROTEA projects). ICDP stands for the International Continental Scientific Drilling Program with UNESCO as a member; DSeis and PROTEA are the abbreviations of the names of the projects "Drilling into Seismogenic zones of M2.0-5.5 earthquakes in South African gold mines (PI: Ogasawara)" and "Probing the heart of an earthquake (a mainshock) and life in the deep subsurface (PI: Yabe)"

The seismogenic zone of the 2014 Orkney M5.5 earthquake, South Africa is the target for both of the DSeis and PROTEA projects target. This M5.5 earthquake took place below the mining horizon (2-3 km depth) of the Moab Khotsong gold mine, about 170 km to WSW of Johannesburg; This M5.5 left-laterally ruptured almost the entire depth range (about 3.5-7.0 km depth) of the West Rand Group (WRG) of the neo-Archean Witwatersrand Supergroup (WSG), supracraton metasedimentary hard-rock formations. WSG is known to have been metamorphosed in greenschist (slightly amphibolite) facies and with protolith of marine pelitic or sand formations and basaltic-andesite lava.

In the Klerksdorp gold field (35km long; 20km wide), the dense seismic reflection survey, followed by drilling from surface to the mining horizon located the Vaal Reef (thin tabular gold reef), exceptionally well-preserved in Central Rand Group above WRG in WSG. This was followed by the dense underground drilling and mapping on the mining horizon, revealing that the stratigraphy above and below the Vaal Reef were consistent over the entire Klerksdorp gold field. This stratigraphy was also much less disturbed than that in other tectonically active zones around the world.

The dense seismic network on the mining horizon elucidated the seismogenic zone of the M5.5 Orkney left-lateral-faulting earthquake, which is atypical of mining-induced normal-faulting M<5 earthquakes on the mining horizons. The accurately located aftershocks enabled the DSeis project to make the following discovery:

- (1) The aftershocks were hosted by a potassium-rich lamprophyre dyke but not by the adjacent, sub-parallel, potassium-poor basaltic dyke.
- (2) Both dykes were more mafic than basalt and cut across WRG rocks (pelitic rock, quartzite, basaltic sills, and basaltic andesite lava) that underwent metamorphism in the greenschist (slightly amphibolite) facies with significant hydrothermal (not epithermal) volatile interaction.
- (3) The presence of 1.2 Ga non-meteoric hypersaline brine strongly suggests that the recovered samples have been preserved with minimal environmental impact near the ground surface.

From 16 to 17 October 2025, the ICDP PROTEA workshop, chaired by Yabe, will summarize the above outcomes and identify exciting scientific goals, as well as a feasible plan for drilling into the main rupture zone of the Orkney earthquakes' mainshock. This talk and another by Fujita et al. at this symposium will detail the workshop's results. The first talk will focus on petrographic and chemical analyses (XRF core scan with tens of  $\mu$ m resolution + EPMA), and Fujita et al. will focus on the interpretation of legacy 3D seismic reflection data.

### Visualization of Seismogenic Zone at the South African Archean Craton using Seismic Attributes

<u>Kaoru Fujita<sup>1, 2</sup></u>, Hiroshi Ogasawara<sup>2</sup>, Masaki Kanao<sup>1, 3</sup>, Jun'ichi Okuno<sup>1, 3</sup>, Takeshi Tsuji<sup>4</sup>

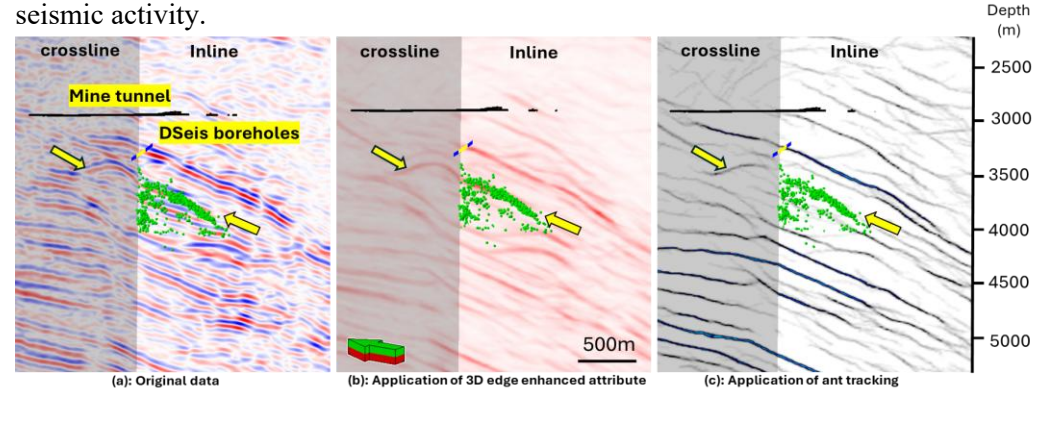
<sup>1</sup>The Graduate University for Advanced Studies, SOKENDAI

<sup>2</sup>Ritsumeikan University, <sup>3</sup>National Institute of Polar Research, <sup>4</sup> The University of Tokyo

Attribute analysis of seismic reflection data is a common technique in the field of oil/gas exploration. This approach enhances and visualizes the continuity and discontinuity of acoustic impedance contrasts (e.g., fault), which are often difficult to discern from seismic volume. It provides a highly effective means for interpreting geological boundaries and faults.

In this study, we applied attribute analysis to the high-resolution 3D seismic reflection data acquired at the Kaapvaal Craton in South Africa, to interpret subsurface geological structures, including stratigraphy and faults. We also evaluated the relationship between the derived information and the actual distribution of seismic activity. Although numerous types of seismic attributes have been proposed, we mainly utilizes attributes that can enhance the geometrical discontinuity. The 3D edge-enhanced attribute was used to extract the continuity of stratigraphic surfaces, while the Chaos Attribute was applied to extract pre-existing faults. Ant Tracking was subsequently applied to each of these attributes. Furthermore, the interpreted stratigraphic boundaries and pre-existing faults were compared with the distribution of aftershocks from the 2014 Orkney earthquake in the same region. This allowed us to examine whether the seismic activity is consistent with specific geological structures.

Previous studies have revealed that streak-like aftershock activity corresponds to strong reflection surfaces (Fujita et al., 2024). In addition, this presentation will highlight the geometric characteristics of strong reflection surfaces associated with streak-like seismic activity (Figure 1). We will also discuss the relationship between pre-existing faults and seismic activity (Figure 2), as well as the influence of subsurface geological structures on



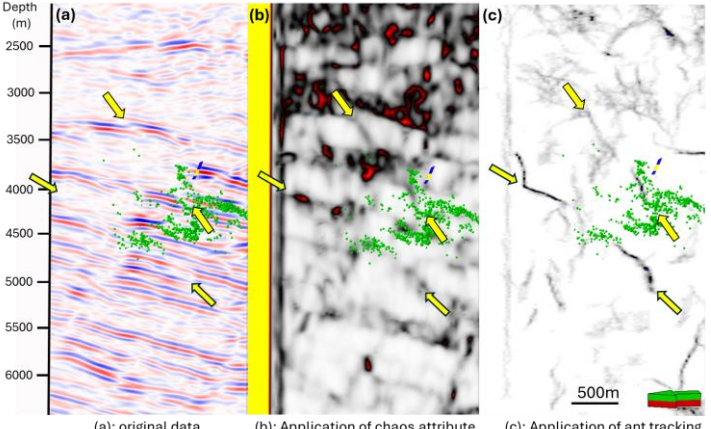


Figure 2. Using Chaos attributes combined with Ant Tracking facilitates the extraction of fault- or fracture-related features. Yellow arrows show pre-existing faults or fractures in the aftershock zones.

Figure 1. The continuity of stratigraphic surfaces is emphasized using the 3D edge-enhanced attribute combined with Ant Tracking facilitates. Crosssections along the hypocenter distribution (Inline) and perpendicular to it (crossline). Green Dots represent aftershockhypocenters determined by the Double-Difference method. Yellow arrows show strong reflectors corresponding to the streak-like aftershock distribution.

### References

Fujita, K., Ogasawara, H., Kanao, M., Tadokoro, R., Horiuchi, S., Okubo, M., Naoi, M., Manzi, M., Suzuki, K., Ogawa, K., and DSeis team, Relocation of hypocenters just around the ICDP DSeis boreholes using the cross-correlation and the Double Difference, JpGU 2024, SSS07-10, Japan, 26-31 May, 2024

### Zircon chronology of Mesoarchaean Ulamertoq ultramafic body, southern West Greenland

Keita Itano<sup>1</sup>, Mami Takehara<sup>2</sup>, Kenji Horie<sup>2</sup>, Ikuya Nishio<sup>3</sup>, Tomoaki Morishita<sup>4</sup>

<sup>1</sup>Akita University

<sup>2</sup>National Institute of Polar Research

<sup>3</sup>Hiroshima University

<sup>4</sup>Kanazawa University

The Akia terrane forms part of the North Atlantic Craton in West Greenland and consists predominantly of Mesoarchean to Neoarchean orthogneisses (e.g., Gardiner et al., 2020). It is dominated by ca. 3000 Ma TTGs (Gardiner et al., 2019), with locally preserved older dioritic bodies (ca. 3220 Ma) (Garde et al., 2000; Gardiner et al., 2019). In recent years, considerable effort has focused on investigating small ultramafic-mafic bodies (UMBs) within the Akia terrane (e.g., Maniitsoq Norite Belt: Waterton et al., 2020; Miaggoq UMB: Zemeny et al., 2023; Seqi UMB: Wang et al., 2024). The origin of these ultramafic bodies—whether they represent ancient mantle fragments or cumulates—remains under debate. Mafic cumulates such as norite associated with peridotite are key to addressing this question. Altough Waterton et al. (2020) revealed that the norite belt in the Maniitsoq Norite Belt records magmatic activity at ca. 3010–3000 Ma, the ages of the norites associated with the peridotite have not yet been directly constrained. This study aims to constrain the emplacement age of t hese mafic cumulates through zircon U–Pb dating.

We recovered zircon grains from the Ulamertoq UMB samples (Table 1). Zircon U–Pb ages were obtained with a sensitive high-resolution ion microprobe (SHRIMP-IIe) at National Institute of Polar Research, following the procedures of Takehara and Horie (2019). In the cathodoluminescence (CL) images, subhedral zircons grains from the norite are characterized by a structure with dark, homogeneous cores and bright mantles/rims (Fig. 1a–b). For the peridotite sample, only two anhedral zircon grains were recovered, showing homogeneous dark and bright domains (Fig. 1c). Zircons from the granite are euhedral and include large grains up to 500  $\mu$ m, but CL images demonstrate clear evidence of secondary disturbance. The U–Pb results indicate that zircons from the norite form two clusters according to their Th/U ratios, with domains of Th/U > 1 and Th/U < 1. For concordant data of the norite samples, the weighted mean ages are as follows: : in sample 56415, the Th/U > 1 domain yielded 3043  $\pm$  7 Ma (n = 8), whereas the Th/U < 1 domain yielded 3006  $\pm$  3 Ma (n = 24); in sample 56421, the Th/U > 1 domain yielded 3056  $\pm$  3 Ma (n = 11), and the Th/U < 1 domain yielded 3016  $\pm$  5 Ma (n = 12). In contrast, zircons from the peridotite, irrespective of their CL characteristics, gave a weighted mean age of 3007  $\pm$  9 Ma (n = 4). Some zircon analyses from the granite were discordant, the others preserved provided a weighted mean age of 2964  $\pm$  2 Ma (n = 24).

The high Th/U domains of the norite zircons, forming older age clusters, suggest crystallization under high-temperature conditions (Kirkland et al., 2015). Thus, the 3040–3050 Ma ages are most likely to record the emplacement of the norite. The younger 3006–3016 Ma low Th/U domains overlap with the  $3007 \pm 9$  Ma peridotite age and with the timing of widespread TTG magmatism in the region. Although further verification through trace element analysis is required, these ages can be interpreted as representing metasomatic alteration of the norite and peridotite by felsic melts. This interpretation is supported by the wide lithological variations in ultramafic rocks caused by multiple metasomatic processes (Nishio et al., 2022). The metasomatic agent was most likely related to ca. 3000-3050 Ma TTG magmatism that was active throughout the Akia terrane, rather than with the granite intrusion  $(2964 \pm 2 \text{ Ma})$  in the peridoteite.

Table 1. Sample information of the studied rocks.

Sample ID	Lithology	Latitude (N)	Longitude (W)
565414	Granitic Pegmatite	64° 54.577	51° 11.763
565415	Norite	64° 54.577	51° 11.763
565440	Peridoite	64° 54.592	51° 11.652
565421	Norite	64° 54.631	51° 11.756

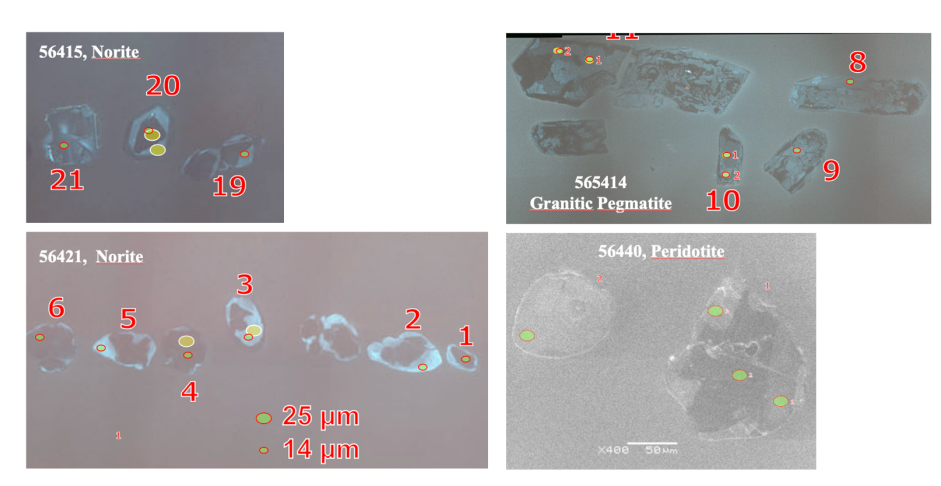


Figure 1. Representative cathodoluminescence images of the studied zircons.

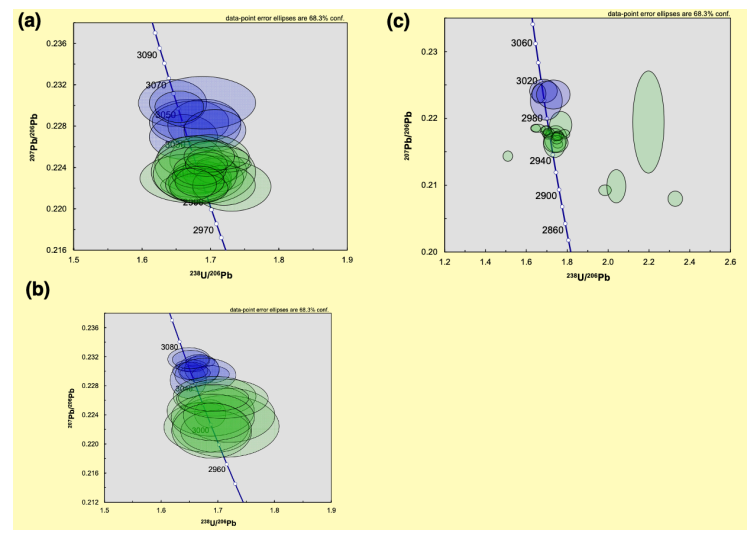


Figure 2. Concordia diagrams of zircons from (a) norite sample 565414, (b) norite sample 565421, and (c) peridotite (565440) and granite (565414).

#### References

Garde AA, Friend CR, Nutman AP et al., Rapid maturation and stabilisation of middle Archaean continental crust: the Akia terrane, southern West Greenland. Bulletin of the Geological Society of Denmark, 47, 1-27, 2000. Gardiner NJ, Kirkland CL, Hollis J, et al., Building mesoarchaean crust upon Eoarchaean roots: the Akia terrane,

West Greenland. Contributions to Mineralogy and Petrology, 174(3), 20, 2019.

Gardiner NJ, Kirkland CL, Hollis J, et al., North Atlantic Craton architecture revealed by kimberlite-hosted crustal zircons. Earth and Planetary Science Letters, 534, 116091, 2020.

Kirkland CL, Smithies RH, Taylor RJM, et al., Zircon Th/U ratios in magmatic environs. Lithos, 212, 397-414, 2015.

Nishio I, Morishita T, Itano K., et al., Metasomatic modification of the Mesoarchaean Ulamertoq ultramafic body, southern West Greenland. Journal of Petrology, 63(3), egac004, 2022.

Takehara M, Horie K, U–Pb zircon geochronology of the Hida gneiss and granites in the Kamioka area, Hida Belt. Island Arc, 28(4), e12303, 2019.

Wang J, Cai P, Yang J, et al., Age and petrogenesis of Archaean chromitite from the Seqi Ultramafic Complex, southern West Greenland. Lithos, 482, 107714, 2024.

Waterton P, Hyde WR, Tusch J, et al., Geodynamic implications of synchronous norite and TTG formation in the 3 Ga Maniitsoq Norite Belt, West Greenland. Frontiers in Earth Science, 8, 562062, 2020.

Zemeny A, Kinney C, Yakymchuk C, et al., Mesoarchaean peridotite-norite cumulates of SW Greenland–The Miaggoq ultramafic complex. Lithos, 458, 107352, 2023.

### Tonian metamorphism in the eastern part of the Prince Olav Coast, East Antarctica

Sotaro Baba<sup>1</sup>, Kenji Horie<sup>2</sup>, Mami Takehara<sup>2</sup>, Nobuhiko Nakano<sup>3</sup>, Shin-ich Kagashima<sup>4</sup>, Tomokazu Hokada<sup>2</sup>, Atsushi Kamei<sup>5</sup>

<sup>1</sup>University of the Ryukyus <sup>2</sup>National Institute of Polar Research <sup>3</sup>Kyushu University <sup>4</sup>Yamagata University <sup>5</sup>Shimane University

The Lützow-Holm Complex, an Ediacaran-Cambrian mobile belt, is distributed in the area extending from eastern Dronning Maud Land (35°E) to western Enderby Land (45°E) in East Antarctica (Hiroi et al., 1991; Shiraishi et al., 1994; 2003). Baba et al. (2022) reported the metamorphic age of amphibolite-facies gneiss from the Akebono Rock on the eastern Prince Olav Coast using a high-sensitivity high-resolution ion microprobe (SHIRIMP). Based on the Ti content and age of zircons, they found that amphibolite-facies metamorphism occurred during the Tonian period, 937 ± 6 Ma. This Tonian metamorphism has also been reported for the Niban Rock, located west of Cape Hinode (Mori et al., 2023; Kitano et al., 2023), suggesting that similar rocks are widely distributed. These results contradict the previous concept that the entire Lützow-Holm Complex underwent regional metamorphism during the Cambrian, with the metamorphic grade increasing progressively from northeast to southwest. There are many unexplored outcrops to the east of the Akebono Rocks, and information on their metamorphism, metamorphic ages, and protoliths is crucial for clarifying the extent and formation processes of metamorphic rocks that exhibit Tonian ages. We report the results of U-Pb zircon dating using SHRIMP on metamorphic rocks exposed in previously unexplored Chijire Rocks (collected by the 63rd Antarctic Research Expedition) and metamorphic rocks exposed at Cape Ryûgû (collected by the 19th Antarctic Research Expedition, Nakai et al., 1980) to the east of them.

No zircons older than 1100 Ma were found in the rock samples from the Chijire Rocks and Cape Ryûgû. Zircon core ages from both exposures are within the range of core ages for the Akebono Rock (1120-1014 Ma, N=26). Zircon rim ages for the two Chijire Rocks samples indicate approximately 970 Ma, inferring a metamorphic age; a similar age was obtained for W419 collected from Cape Ryûgû (low Th/U zircon core and mantle: 984±5 Ma). For the two samples from Cape Ryûgû, many of the zircon rims plotted around approximately 545 Ma, which is considered a major metamorphic age. These dating results confirm Tonian metamorphism in the Chijire Rocks and Cape Ryûgû, indicating that Cape Ryûgû underwent intense metamorphic reworking around 545 Ma. The basement rocks that underwent metamorphism in the Tonian are distributed over an area of approximately 90 km from Niban Rock to Cape Ryûgû, via Cape Hinode, Akebono Rock, and Chijiri Rocks. It is thought that Niban Rock at the western end (Mori et al., 2023; Kitano et al., 2023) and Cape Ryûgû at the eastern end were reworked in the Cambrian. We propose that these areas can be subdivided as "Tonian Prince Olav Terrene" in the Lützow-Holm Complex.

#### References

Baba et al. (2022) Gondwana Res. 105, 243–261. Hiroi et al. (1991) Geological Evolution of Antarctica, Cambridge University Pres, 83-87. Kitano et al. (2023) J. Min. Petrol. Sci. 118, S009. Mori et al. (2023) J. Min. Petrol. Sci., 118, S005. Nakai et al. (1980) Antarctic Geological Map Series Sheet 15, Cape Ryûgû. Shiraishi et al. (1994) Journal of Geology, 102, 47–65. Shiraishi et al. (2003) Polar Geosci., 16, 76-99.

# Contrastive *P-T* paths and tectonic impliation of intermediate to mafic gneisses from Akebono Rock in the Lützow-Holm Complex, East Antarctica

Ippei Kitano<sup>1</sup>, Tomokazu Hokada<sup>2</sup>, Sotaro Baba<sup>3</sup>, Atsushi Kamei<sup>4</sup> and Yoichi Motoyoshi<sup>2</sup>

<sup>1</sup> The Hokkaido University Museum

<sup>2</sup> National Institute of Polar Research

<sup>3</sup> University of the Ryukyus

<sup>4</sup> Shimane University

The Lützow-Holm Complex (LHC) in East Antarctica is composed of Ediacaran to Cambrian metamorphic rocks and intrusive rocks, except for some Tonian metamorphic rocks around Cape Hinode (e.g., Motoyoshi et al., 2004; Hiori et al., 2006; Dunkley, 2020). The former has been divided traditionally into amphibolite-facies, transitional and granulite-facies zones from northeast to southwest (e.g., Hiroi et al., 1983; Shiraishi et al., 1994). Tonian metamorphic rocks have been also identified from Niban-nishi Rock (Kitano et al., 2023; Mori et al., 2023), Akebono Rock (Baba et al., 2022; Kitano et al., 2023) and Cape Hinode (Dunkley, 2020) with amphibolite- to granulite-facies grade within traditional amphibolite-facies zone in the northeast LHC. However, the tectonic evolution of Tonian metamoprhism remains obscure. Akebono Rock consisits of amphibolite-facies metamorphosed rocks of biotite gneiss, garnet-biotite gneiss, biotite-hornblende gneiss, calc-silicate rock and amphibolite intruded by granite, pegmatite and slightly recrystallized basaltic to andesitic dyke (Hiroi et al., 1986). Baba et al. (2020, 2022) revealed a clockwise pressure (P)-temperature (T) paths with the peak condition of ca. 6–8 kbar and 700 °C at ca. 940 Ma from pelitic gneisses and amphibolites in western Akebono Rock. On the other hand, Kitano et al. (2024) reported an anti-clockwise P-T path with the peak condition of ca. 5–8 kbar and 590–660 °C from a staurolite-bearing mafic gneiss at ca. 930 Ma (Kitano et al., 2023) in eastern Akebono Rock. Thus, the understanding of their special relation between rocks showing the clockwise and anti-clockwise P-T paths is a key issue to decipher the metamorphic evolution in this area as well as Tonian metamorphic region in the LHC. This study reports petrographic features of intermediate to mafic gneisses focused on the occurrences of epidote and P-T paths between the west and east Akebono Rocks.

Those gneisses in Akebono Rock occur as interlayers alternating with felsic gneisses or blocks within them. Although no reports of epidote from mafic metamorphic rocks from Akebono Rock, two modes of occurrences of epidote were identified in present study. One is the euhedral to subhedral and fine- to medium-grain in the matrix replacing hornblende with quartz as a secondary phase occasionally coexisting with garnet. The other is the subhedral to anhedral fine-grained inclusion in plagioclase or garnet as a relic phase with or without allanite. The former and latter are observable from the intermediate to mafic gneisses in central to eastern and western Akebono Rock, respectively. The subhedral to anhedral garnet porphyroblasts of that from the central part have the increase of Ca contents toward rim with inclusions of biotite + plagioclase + quartz ± epidote ± ilmenite ± titanite and minor occurrences of epidote as inclusions in high-Ca garnet rim or secondary phases replacing hornblende in the matrix. On the other hand, those garnets from the western part show oscillatory zoning patterns of Ca contents. They gradually change with increasing from core to mantle, decreasing to the inner rim, and increasing to the marginal outer rim. The inclusions of hornblende  $\pm$  biotite  $\pm$  plagioclase  $\pm$  quartz  $\pm$  K-feldspar  $\pm$  muscovite  $\pm$  albite  $\pm$  epidote  $\pm$ ilmenite ± titanite are present. Relic epidote occur in plagioclase with allanite core or garnet mantle to inner rim. Applying to geothermobarometries and petrogenetic grids for inclusions in garnet porphyroblasts and matrix phases yielded the anticlockwise P-T path for the gneiss from the central part and the clockwise one for that from the western part. The contrastive P-T paths deduced by this study and previous studies possibly indicate different tectono-thermal histories between the central to eastern and western Akebono Rock. The discrepancies of dominant lithologies and intrusive phases (Hiroi et al., 1986), deformation and magmatic histories (Baba et al., 2020) between the eastern and western regions may support our ideas. In view of lithologies, metamorphic grades and detrital zircon ages, Tonian metamorphic region of Niban Rock, Akebono Rock, and Cape Hinode is likely to have the variation. It may indicagte the region is a collage of small terranes amalgamted during Tonian. However, the further database of metamorphic petrology, geochemistry and geochronology in this region is required to clarify it.

#### References

Baba S., Hokada, T., Kamei, A., Kitano, I., Motoyoshi, Y., Nantasin, P., Setiawan, N.I. and Dashbaatar, D., Tectonometamorphic evolution and significance of shear-zone lithologies in Akebono Rock, Lützow-Holm Complex, East Antarctica. Antarctic Science, 33, 1, 52–72, 2020.

- Baba, S., Horie, K., Hokada, T., Takehara, M., Kamei, A., Kitano, I., Motoyoshi, Y., Nantasin, P., Setiawan, N.I., and Dashbaatar, D., Newly found Tonian metamorphism in Akebono Rock, eastern Dronning Maud Land, East Antarctica. Gondwana Research, 105, 243–261, 2022.
- Dunkley, D., Hokada, T., Shiraishi, K., Hiroi, Y., Nogi, Y. and Motoyoshi, Y., Geologica subdivision of the Lützow–Holm Complex in East Antarctica: from the Neoarchean to the Neoproterozoic. Polar Science, 26, 100606, 2020.
- Hiroi, Y., Shraishi, K., Yanai, K. and Kizaki, K., Aluminum slicates in the Prince Olav and Sôya Coasts, East Antarctica. Memoirs of National Institute of Polar Research, Special issue, 28, 115–131, 1983.
- Hiroi, Y., Shraishi, K. and Sasaki, K., Explanatory text of geological map of Akebono Rock, Antarctica. Antarctic Geologicai Map Series, Sheet 16 Akebono Rock. NIPR, Tokyo, 1986.
- Hiroi, Y., Motoyoshi, Y., Satish-Kumar, M., Kagashima, S., Suda, Y. and Ishikawa, N., Granulites from Cape Hinode in the amphibolite-facies eastern part of Prince Olav Coast, East Antarctica: New evidence for allochthonous block in the Lützow-Holm Complex. Polar Geoscince, 19, 89–108, 2006.
- Kitano, I., Hokada, T., Baba, S., Kamei, A., Motoyoshi, Y., Nantasin, P., Setiawan, N.I., Dashbaatar, D., Toyoshima, T., Ishikawa, M., Katori, T. Osanai, Y. and Nakano, N. Zircon geochronology of high-grade metamorphic rocks from outcrops along the Prince Olav Coast, East Antarctica: Implications for the multi-thermal events and regional correlations. Journal of Mineralogical and Petrological Sciences, 118, ANTARCTICA, S009, 2023.
- Kitano, I., Hokada, T., Baba, S., Kamei, A., Motoyoshi, Y., *P*–*T* path of a staurolite-bearing gneiss from eastern Akebono Rock in the Lützow-Holm Complex, East Antarctica. The 131st Annual Meeting of the Geological Society of Japan, Abstract, 2024.
- Mori, Y., Hokada, T., Miyamoto, T., Ikeda, T., Metamorphic age and pressure-temperature conditions recorded in a sillimanite-garnet-bearing pelitic gneiss from Niban-nishi Rock of Niban Rock on the Prince Olav Coast, eastern Dronning Maud Land, East Antarctica: Evidence for Tonian metamorphism. Journal of Mineralogical and Petrological Sciences, 118, ANTARCTICA, S005, 2023.
- Motoyoshi, Y., Hokada, T., Hiroi, Y. and Shiraishi, K., EMP dating on Cape Hinode of the Lützow-Holm Complex, East Antarctica. The 24th Symposium on Antarctic Geosciences, Abstract, NIPR, Tokyo, 2004.
- Shiraishi, K., Ellis, D.J., Hiroi, Y., Fanning, C.M., Motoyoshi, Y. and Nakai, Y., Cambrian orogenic belt in East Antarctica and Sri Lanka: implication for Gondwana assembly. Journal of Geology, 102, 47–65, 1994.

# The relation between garnet composition and *P-T-X-f*<sub>O2</sub> conditions: Example from calc-silicate granulite from Rundvågshetta, Lützow-Holm Complex, East Antarctica

Koyomi Abe<sup>1</sup>, Madhusoodhan Satish-Kumar<sup>1</sup>, Tomokazu Hokada<sup>2</sup>, Krishnan Sajeev<sup>3</sup>, and James A. D. Connolly<sup>4</sup>

<sup>1</sup>Niigata University

<sup>2</sup>National Institute of Polar Research

<sup>3</sup>Indian Institute of Science

<sup>4</sup>ETH Zurich

Calc-silicate rocks play an important role in reconstructing the pressure-temperature-fluid (*P-T*-fluid) history because their mineral assemblages extremely sensitive to interactions with fluids. Garnet, which is an almost ubiquitous phase in these rocks, has been suggested to possess composition that reflect not only *P-T* conditions, but also fluid as well as oxygen fugacity conditions (Dasgupta and Pal, 2005). Despite this, there are limited studies that have comprehensively examined garnet disequilibrium textures, its compositional changes and the associated fluid conditions. In this study, calc-silicate granulite from Rundvågshetta, Lützow-Holm Complex is studied to investigate the factors controlling compositional variations and texture of garnet. By doing so we could also estimate the changing *P-T*-fluid evolution in this region.

The Lützow-Holm Complex of East Antarctica experienced high- to ultrahigh-temperature metamorphism and is characterized by an increase in metamorphic grade from amphibolite facies in the northeast to granulite facies in the southwest region, reaching the peak thermal condition at Rundvågshetta. The *P-T* conditions of Rundvågshetta have been estimated by previous studies to be > 900°C, 10–13 kbar (e.g. Motoyoshi and Ishikawa, 1997; Yoshimura et al., 2008; Suzuki et al., 2025). We examined calc-silicate granulite occurring as a block surrounded by pyroxene gneiss (Satish-Kumar et al., 2006).

The calc-silicate granulite shows granoblastic texture and contains garnet, clinopyroxene, scapolite, plagioclase and quartz with accessory calcite, titanite and apatite. Three domains can be distinguished by mineral modes; Grtabsent domain, Scp-rich domain and Pl-rich domain. In the latter two domains, scapolite and plagioclase exhibit marked differences in modal abundance. Garnet grains contain inclusions of clinopyroxene, scapolite, plagioclase, calcite and quartz, indicating that garnet has grown at the expense of these minerals. At places, porphyroblastic garnet and quartz are present, and their interface is characterized by intergrown appendages. Coronal garnet, which was recognized as a retrograde metamorphic texture, are also present. In addition, prehnite occurs surrounding scapolite, indicating an influx of  $H_2O$ -rich fluid during low temperature retrograde stage. Mineral compositions determined by EPMA indicate that garnet has a grossular–andradite solid solution and granular garnet is rich in the grossular content ( $Fe^{3+}/(Fe^{3+}+AI) = 0.10-0.20$ ). On the other hand, coronal garnet are rich in andradite content up to  $Fe^{3+}/(Fe^{3+}+AI) = 0.44$ .

Phase equilibria modeling was conducted to estimate the peak condition for both Scp-rich domain and Pl-rich domain, yielding results consistent with the P-T range reported in the previous studies. This suggests that the calc-silicate rocks and their enclosing host rocks underwent metamorphism under the same conditions. Additionally, T-X<sub>CO2</sub> diagram indicates that the three domains formed under different X<sub>CO2</sub> conditions, implying that during peak metamorphism, spatial heterogeneities in X<sub>CO2</sub> at the scale of several centimeters existed within the calc-silicate rock. The formation of andradite-rich coronal garnet has been discussed to depend on temperature and oxygen fugacity (Dasgupta and Pal, 2005). This study highlights that the necessity of taking into account both temperature and fluid characteristics including oxygen fugacity to discuss the origin of andradite-rich coronal garnet.

#### References

Dasgupta, S. and Pal, S. (2005) Origin of grandite garnet in calc-silicate granulites: mineral fluid equilibria and petrogenetic grids. Journal of Petrology, 46, 1045–1076.

Motoyoshi, Y. and Ishikawa, M. (1997) Metamorphic and structural evolution of granulites from Rundvågshetta, Lützow-Holm Bay, East Antarctica. ed. by C.A. Ricci. Siena, Terra Antarctica. Publ., 65–72.

- Satish-Kumar, M., Motoyoshi, Y., Suda, Y., Hiroi, Y. and Kagashima, S. (2006) Calc-silicate rocks and marbles from Lützow-Holm Complex, East Antarctica, with special reference to the mineralogy and geochemical characteristics of calc-silicate mega-boudins from Rundvågshetta. Polar Geoscience, 19, 37–61.
- Suzuki, K., Kawakami, T., Kogiso, T., Sakata, S., et al. (2025) Tectonic setting and evolution of Anatectic melt composition during prograde metamorphism up to UHT metamorphism: constraints from P-T-t-melting path from Rundvågshetta, Lützow-Holm Complex, East Antarctica. Journal of Metamorphic Geology, 43, 467–495.
- Yoshimura, Y., Motoyoshi, Y. and Miyamoto, T. (2008) Sapphirine + quartz association in garnet: implication for ultrahigh-temperature metamorphism at Rundvågshetta, Lützow Holm Complex, East Antarctica. Geological Society, London, Special Publications, 308 (1), 377–390.

# High-Zr rutiles as evidence for ultrahigh-temperature metamorphism in a garnet-biotite gneiss from Brattnipene, Sør Rondane Mountains, East Antarctica

<u>Hiroto Gondo</u><sup>1</sup>, Tetsuo Kawakami<sup>1</sup>, Fumiko Higashino<sup>1</sup>, Tatsuro Adachi<sup>2</sup> and Masaoki Uno<sup>3</sup>

<sup>1</sup>Kyoto University, <sup>2</sup>Kyusyu University, <sup>3</sup>The University of Tokyo

Ultrahigh-temperature metamorphism (UHTM) is defined as regional metamorphism that occurs at temperatures exceeding 900°C, typically under pressures at or below the sillimanite–kyanite transition line (Harley, 2021). Understanding the spatial extent and duration of UHTM is crucial for reconstructing the formation processes of the associated UHTM rocks. The Sør Rondane Mountains (SRM) in eastern Dronning Maud Land, East Antarctica, are composed predominantly of high-grade metamorphic rocks ranging from amphibolite to granulite facies (Shiraishi et al., 1997), and are structurally divided into northeastern (NE) and southwestern (SW) terranes by the Main Tectonic Boundary (MTB; Osanai et al., 2013). Although some UHTM rocks have been found in large moraines or talus deposits from both terranes (Nakano et al., 2011; Baba et al., 2019), their outcrops are limited to the NE terrane so far and the spatiotemporal extent of UHTM in the SRM remains unclear (Higashino and Kawakami, 2022; Satish-Kumar et al., 2025). In this study, we report the mode of occurrence of rutile with high Zr concentrations in a pelitic gneiss collected from Koyubi Ridge, Brattnipene from the SW terrane. We further discuss the possible UHTM recorded in the studied gneiss.

The studied garnet-biotite gneiss consists of quartz-rich and quartz-poor layers, a leucogranite vein, and a planar biotite-filling crack. The gneissose structure defined by the quartz-rich and quartz-poor layers is crosscut by the leucogranite vein, suggesting that the vein intruded after the formation of the gneissose structure. The leucogranite vein is further deformed by the same ductile deformation as the gneissose structure, evidenced by the fabric of the vein concordant with the gneissose structure. The biotite-filling crack cuts the entire rock fabric.

The quartz-rich layers are composed mainly of garnet porphyroblasts, quartz, plagioclase (An24-29), biotite, rutile, and ilmenite. Most of the rutile grains in the matrix are partially replaced by ilmenite. The Zr concentration of rutile in the matrix is below 1303 ppm. The garnet porphyroblasts include quartz, plagioclase, biotite, rutile, and zircon, and exhibit oscillatory zoning in phosphorus. Rutile is included in garnet as (i) a single phase (Zr = 1510-3790 ppm; Nb = 529-886 ppm), (ii) polyphase inclusion of biotite + rutile (Zr = 170–1118 ppm; Nb = 249-12841 ppm) + quartz, and (iii) rutile (Zr = 3546-7633 ppm; Nb  $\leq$  62 ppm) + quartz. Type (i) and (iii) rutile grains are subhedral to euhedral and fine-grained (<20  $\mu$ m), whereas type (ii) rutile grains are anhedral and coarse-grained (<100  $\mu$ m). Most of the type (ii) rutile grains do not exhibit zoning in Zr and Nb. Although a few grains show a decrease in both Zr and Nb towards the rim, no high-Zr rims or domains were observed in type (ii) rutile grains. Zoning in type (i) and (iii) rutile grains was not investigated because of their fine grain size. These three types are found as inclusions throughout the garnet, and phosphorus zoning shows that all rutile grains are included on the isochronous surfaces that also include zircon and quartz.

The quartz-poor layers consist mainly of garnet porphyroblasts, plagioclase (An31-37), biotite, sillimanite, spinel, rutile, and ilmenite, and are characterized by the presence of spinel and a marked deficiency of quartz. Rutile in the matrix (Zr = 311-1792 ppm) occurs either as a single phase or as grains partially replaced by ilmenite. No significant difference in Zr concentration was observed between rutile grains with and without ilmenite replacement. Plagioclase in the matrix shows a core (An31-32) hosting randomly oriented rutile needles, and a rim (An33-37) that includes zircon and rutile (Zr = 1044-1229 ppm; Nb = 4446-7244 ppm). The garnet porphyroblasts (3-5 mm) include plagioclase, biotite, sillimanite, spinel, rutile, and zircon, and lack oscillatory zoning in phosphorus. Discontinuous Ca zoning defines a garnet core (Grs3-4) and rim (Grs4-5). The rim exhibits a spotted Ca zoning pattern, characterized by multiple domains (<1 mm) in which Ca decreases toward the outer edge. The inclusion mineral assemblage in garnet does not change from core to rim, while spinel inclusions tend to be coarser in the rim. Rutile in garnet occurs as (i) a single phase (Zr = 148-1525 ppm; Nb = 295-29226 ppm), (ii) polyphase inclusions of biotite + rutile (Zr = 141-3450 ppm; Nb = 451-7011 ppm), and (iii) spinel/sillimanite + rutile (Zr = 3428-7707 ppm; Nb = 3793-30175 ppm). Type (ii) and Type (iii) rutile grains are included both in core and rim, whereas Type (i) is included only in the rim. All quartz inclusions are polyphase and single phase quartz inclusions are absent.

A rutile grain (Zr = 7633 ppm) included in garnet from the quartz-rich layer is in contact with quartz, and zircon is also present on the same isochronous surface based on P oscillatory zoning, indicating that rutile, quartz, and zircon coexisted in equilibrium. Applying the Zr-in-rutile geothermometer (Tomkins et al., 2007) to this rutile gave UHT condition over 952°C, although the pressure is not constrained. In contrast, garnet cores from the quartz-poor layer include only rutile and zircon and lack quartz. By assuming aSiO<sub>2</sub>= 0.5, Zr-in-rutile geothermometer (Ferry and Watson, 2007) yielded 849-971°C (Zr = 7707 ppm) under the pressure condition of the sillimanite stability field (P < 14 kbar). These results suggest that at least part of the

garnet growth occurred under UHT conditions, indicating that UHTM is not limited to the NE terrane but may also extend to the SW terrane. Mixed occurrences of UHT and non-UHT rutiles included in a single garnet grain suggest the possibility of polymetamorphism. Dating the UHT and non-UHT rutiles would be a clue to understand the complexity of this sample and timing of the UHTM in the SRM.

#### References

- Baba, S., Osanai, Y., Adachi, T., et al., Metamorphic P-T conditions and variation of REE between two garnet generations from granulites in the Sør Rondane Mountains, East Antarctica. Mineralogy and Petrology, 113, 821–845, 2019.
- Ferry, J.M., Watson, E.B., New thermodynamic models and revised calibrations for the Ti-in-zircon and Zr-in-rutile thermometers. Contributions to Mineralogy and Petrology, 154, 429–437, 2007.
- Harley, S.L., UHT metamorphism. In: Alderton, D. & Elias, S.A. (eds), Encyclopedia of Geology. Elsevier, 522-552, 2021.
- Higashino, F., Kawakami, T., Ultrahigh-temperature metamorphism and melt inclusions from the Sør Rondane Mountains, East Antarctica. Journal of Mineralogical and Petrological Sciences, 117, 10, 2022.
- Nakano, N., Osanai, Y., Baba, S., Adachi, T., Hokada, T., Toyoshima, T., Inferred ultrahigh-temperature metamorphism of amphibolitized olivine granulite from the Sør Rondane Mountains, East Antarctica. Polar Science, 5, 345–359, 2011.
- Osanai, Y., Nogi, Y., Baba, S., Nakano, N., Adachi, T., Hokada, T., Toyoshima, T., Owada, M., Satish-Kumar, M., Kamei, A., Kitano, I., Geologic evolution of the Sør Rondane Mountains, East Antarctica: collision tectonics proposed based on metamorphic processes and magnetic anomalies. Precambrian Research, 234, 8–29, 2013.
- Satish-Kumar, M., Kiran, S., Higashino, F., Kawakami, T., Hokada, T., Identification of multiple thermal events in high-grade metacarbonate rocks using carbon isotope thermometry: an example from the Sør Rondane Mountains, East Antarctica. Geological Journal, 60, 455–483, 2025.
- Shiraishi, K., Osanai, Y., Ishizuka, H., Asami, M., Geological map of the Sør Rondane Mountains, Antarctica. Antarctic Geological Map Series, Sheet 35, scale 1:250,000. National Institute of Polar Research, Tokyo, 1997.
- Tomkins, H.S., Powell, R., Ellis, D.J., The pressure dependence of the zirconium-in-rutile thermometer. Journal of Metamorphic Geology, 25, 703–713, 2007.

# Estimating the radiogenic heat production of metamorphic rocks in Lützow Holm Complex, East Antarctica by Gamma-ray Spectrometry

Devika S. Panicker<sup>1</sup>, Jun Goto<sup>2</sup>, Tomokazu Hokada<sup>3</sup>, Toshiro Takahashi<sup>4</sup> and Madhusoodhan Satish-Kumar<sup>4</sup>

<sup>1</sup>Graduate School of Science and Technology, Niigata University, Japan. <sup>2</sup> Institute for Research Administration, Niigata

University, Niigata, Japan. <sup>3</sup> National Institute of Polar Research, Tokyo 190–8518, Japan. <sup>4</sup> Department of Geology, Faculty

of Science, Niigata University, Japan.

The Lützow-Holm Complex (LHC) in East Antarctica is part of the Neoproterozoic—Cambrian high-grade metamorphic belt within the East African—Antarctic Orogen. The rocks, which underwent amphibolite- to granulite-facies metamorphism during ~600–530 Ma, preserve critical information about the thermal and tectonic evolution of supercontinent Gondwana. Despite its geological significance, systematic studies on natural radioactivity and lithology-dependent radiogenic heat production (RHP) are scarce. Understanding RHP is essential for constraining geothermal heat flow, lithospheric thermal regimes, and Antarctic tectonothermal history. This study aims to quantify natural radioactivity and associated RHP in major lithologies of the Lützow-Holm Complex (LHC) and to assess lithology-specific variations, thereby filling a critical data gap for Antarctic heat flow studies. Determining radioactive heat production in this region is also important for evaluating the current thermal state of Antarctica and for reconstructing the past thermal regime of Gondwana.

A total of 50 representative bedrock samples from the Lützow-Holm Complex (LHC) area were analyzed, and uranium (U), thorium (Th), and potassium (K) concentrations were measured using high-resolution gamma-ray spectrometry, supplemented by geochemical analyses. The lithologies include investigated felsic intermediate orthogneisses (e.g., charnockite, biotite-hornblende gneiss, dioritic gneiss, metagranite), metasedimentary rocks (pelitic and psammitic gneisses, quartzite, marble), metabasites (mafic granulite, amphibolite, ultramafic rocks). Radiogenic heat production was calculated from measured radioelement concentrations. According to the present dataset, radiogenic heat production (RHP) values range from 0.12 to 11.87  $\mu$ W/m<sup>3</sup>. The majority of samples fall below 2 µW/m³, with a smaller subset

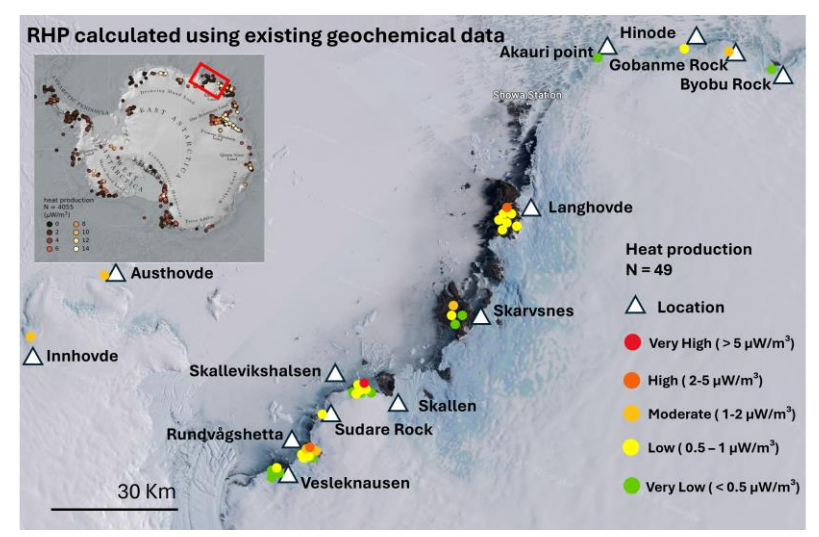


Figure 1: Radioactive heat production calculated in LHC by both geochemical data sets and gamma-ray spectrometry.

in the intermediate range (2–5  $\mu$ W/m³), and with exception of exceeding 5  $\mu$ W/m³ from a granitic occurrence. This variability correlates strongly with mineralogical composition and radioelement distribution.

Comparison with previously published geochemical datasets confirms significant variations within tectonometamorphic domains and among different lithologies, underscoring the importance of direct, high-resolution measurements for accurate RHP estimation. This study provides the first comprehensive dataset of radiogenic heat production (RHP) in the Lützow-Holm Complex (LHC) region, contributing to the development of Antarctic heat production maps. The findings enhance understanding of lithospheric thermal structure, support geothermal heat flow modeling, and serve as a reference for future geochemical and geophysical studies in high-grade metamorphic terrains. Detailed heat production mapping is essential not only for scientific research but also for evaluating potential geothermal energy resources in Antarctic regions. Moreover, an additional 30 samples are currently under analysis, and the extended dataset will be presented at the forthcoming conference.

# Microblock amalgamation and multiphase deformation in the eastern Lützow-Holm Complex, East Antarctica

L. Sreehari<sup>1</sup>, T. Adachi<sup>2</sup>, Y. Mori<sup>3</sup> and T. Hokada<sup>4</sup>

<sup>1</sup>Shimane University,

<sup>2</sup>Kyushu University,

<sup>3</sup>University of Hyogo,

<sup>4</sup>NIPR

The Lützow-Holm Complex (LHC) of East Antarctica records metamorphism from amphibolite to ultrahigh-temperature conditions, providing a key archive for tracing Precambrian tectono-thermal evolution. As part of the East Antarctic Shield, it preserves evidence for crustal growth and reworking from the Archean through the Proterozoic. Recent geochronological work has demonstrated two prominent metamorphic episodes at ca. 1000 Ma and ca. 600 Ma (Dunkley et al., 2020; Baba et al., 2022; Mori et al., 2023). Disentangling the structural links among terranes of different age is therefore essential to unravel their tectonic history.

This study compares structural and lithological relationships at two eastern LHC localities-Kasumi Rock and Niban Rock-through field mapping, aerial imagery, and microstructural analysis. Niban Rock (~3 km²), situated 15 km northeast of Syowa Station, is dominated by biotite gneiss, sillimanite—garnet gneiss, amphibolite, and intruding granites and pegmatites. Amphibolite enclaves within gneisses and granitic intrusions define a polyphase structural record. Three deformation stages are identified: (1) D1 upright folds and reverse shear zones with NW–SE to N–S axial planes, (2) D2 folds with E–W orientations, and (3) D3 dextral strike-slip faults trending NW–SE.

Kasumi Rock (~2 km²), located ~130 km northeast of Syowa Station, exposes biotite and pink gneisses, amphibolite, marble, skarn, minor ultramafic lenses, and distinctive pegmatites with megacrystic K-feldspar. Pegmatite generations provide a relative chronology: early intrusions broadly parallel to gneissic foliation and late cross-cutting dykes representing the youngest igneous phase. Unlike Niban Rock, early deformation is dominated by E–W recumbent folds subsequently refolded into upright, non-coaxial structures, with mineral lineations aligned to fold axes, suggesting progressive deformation.

Microstructural observations from the reverse shear zones at Niban Rock show asymmetrical granitic melt lenses and sigma-type garnet porphyroclasts, indicating top-to-the NE shear. In migmatitic domains, leucocratic layers contain elongated and deformed plagioclase and K-feldspar, whereas melanocratic bands preserve asymmetric garnet. Biotite commonly aligns parallel to foliation within the shear zones, reflecting retrograde recrystallization, while sillimanite grains occur without a preferred orientation. This poster highlights these microstructural features together with regional deformation patterns to illustrate the complex tectono-metamorphic evolution of the locality.

# Long-lived high-grade metamorphism in the Lützow-Holm Complex, East Antarctica: New insights from the combination of monazite Th-U-total Pb and zircon U-Pb geochronology

Haruto Sasaki<sup>1</sup>, Toshiaki Tsunogae<sup>2</sup>

<sup>1</sup>College of Geosciences, University of Tsukuba, Japan

<sup>2</sup>Institute of Life and Environmental Sciences, University of Tsukuba, Japan

Numerous geochronological constraints have been obtained in the context of supercontinent research. The Gondwana Supercontinent is inferred to have formed through complex processes of subduction, accretion, and collision associated with multiple metamorphic events during its amalgamation in the Latest Neoproterozoic (ca. 600-530 Ma) (Meert, 2003). The Lützow-Holm Complex (LHC) in East Antarctica is mainly composed of high-grade metamorphic rocks, and its metamorphic grade is thought to increase continuously from amphibolite facies in the northeast to granulite facies in the southwest (Shiraishi et al., 1994; Hiroi et al., 1991). There have been many geochronological studies performed for the LHC. For example, Hokada et al. (2006) reported Th-U-total Pb monazite ages of 560-500 Ma and 650-580 Ma from Skallen, and inferred the younger age as the timing of peak metamorphism, and older ages as the timing of monazite growth before the peak event. Takahashi et al. (2018) obtained metamorphic ages in the range of 650-510 Ma based on LA-ICP-MS U-Pb zircon from Austhovde, Telen, Skallevikshalsen, and Skallen. Kitano et al. (2023) reported LA-ICP-MS zircon U-Pb ages of 620-530 Ma from Tenmondai Rock, and suggested that the main metamorphic episode in the LHC is likely to be subdivided into three stages: a preceding thermal event (either independent single metamorphic event or prograde stage) at pre-580 Ma, near-peak condition stage during 580-550 Ma, and subsequent retrograde stage after 550 Ma. Therefore, a wide range of ages has been reported for the Neoproterozoic high-grade metamorphism of the LHC, suggesting that the metamorphism extended over tens to hundreds of millions of years. However, the detailed pressure-temperature-time (P-T-t) path of this long-lived metamorphism remains poorly understood. Recently, Takamura et al. (2020) estimated the duration of high-grade metamorphism based on LA-ICP-MS U-Pb ages and REE patterns of zircons from Tenmondai Rock (amphibolite facies) and Sudare Rock (granulite facies). They obtained magmatic ages of >808 Ma (Tenmondai Rock) and >783 Ma (Sudare Rock) during the Mid-Neoproterozoic, and metamorphic ages of 630-481 Ma during the Late Neoproterozoic to Cambrian. Zircons with relatively low Th/U ratios from spots with minimal Pb loss yielded ages of 545-510 Ma from Tenmondai Rock and 555-540 Ma from Sudare Rock. These younger zircons (560-510 Ma) indicate enrichment in HREE and negative Eu anomalies. Combined with the symplectite textures observed around garnet in metabasites, Takamura et al. (2020) suggested that the zircon growth concurrents with garnet consumption, which leads to the interpretation that decompression of the LHC after the peak metamorphism started at 560 Ma.

In this study, we conducted in-situ Th–U-total Pb dating of monazite and uraninite from metamorphic rocks collected across the LHC, with uraninite only from Tenmondai Rock and Sudare Rock. This method allows petrographic observation of dated minerals and their mineral assemblages in thin sections, which was not performed in Takamura et al. (2020). By integrating our results with zircon U–Pb ages reported by Takamura et al. (2020), we attempt to reconstruct the *P*–*T*-*t* path of the LHC. This integration of monazite and zircon geochronology will deepen our understanding of the prolonged high-grade metamorphism recorded in the LHC. Taylor et al. (2014) constrained the age of peak metamorphism based on SHRIMP U–Pb dating of monazite and zircon from the Trivandrum Block in southern India. They inferred that high-grade metamorphism occurred between the growth of metamorphic monazite and the growth of metamorphic zircon. Also, Kadowaki et al. (2019) discussed *P*–*T*-*t* path and long-lived (>90 Myrs) high-grade metamorphism of the Trivandrum Block based on LA-ICP-MS U–Pb dating of monazite and zircon. The obtained ages include 570–540 Ma from Tenmondai Rock, 570–500 Ma from Sudare Rock, 490–420 Ma and 590–550 Ma from Telen, and 500–440 Ma from Austhovde. These ages are compared with zircon U–Pb ages reported by Takamura et al. (2020). Our monazite ages suggest the timing of high-grade metamorphism as 560–510 Ma which is consistent with the zircon ages of the same regions reported in previous studies including Takamura et al. (2020). We also obtained post-peak ages of <500 Ma for monazites intergrowing with retrograde biotite, possibly suggesting the timing of fluid infiltration during exhumation.

#### References

Hiroi, Y., Shiraishi, K., Motoyoshi, Y., 1991. Late Proterozoic paired metamorphic complexes in East Antarctica, with special reference to the tectonic significance of ultramafic rocks. In: Thomson, M.R.A., Crame, J.A., Thomson, J.W. (Eds.), Geological Evolution of Antarctica. Cambridge University Press, Cambridge, 83–87.

- Hokada, T., Motoyoshi, Y., 2006. Electron microprobe technique for U-Th-Pb and REE chemistry of monazite, and its implications for pre-, peak- and postmetamorphic events of the Lützow-Holm Complex and the Napier Complex, East Antarctica. Polar Geosciences 19, 118-151.
- Kadowaki, H., Tsunogae, T., He, X.F., Santosh, M., Takamura, Y., Shaji, E., Tsutsumi, Y., 2019. Pressure-temperature-time evolution of ultrahigh-temperature granulites from the Trivandrum Block, southern India: implications for long-lived high-grade metamorphism. Geological Journal 54, 3041–3059.
- Kitano, I., Hokada, T., Baba, S., Kamei, A., Motoyoshi, Y., 2023. Zircon geochronology of high-grade metamorphic rocks from outcrops along the Prince Olav Coast, East Antarctica: Implications for multi-thermal events and regional correlations. Journal of Mineralogical and Petrological Sciences 118, S009.
- Meert, J., 2003. A synopsis of events related to the assembly of eastern Gondwana Tectonophysics 362, 1–40.
- Shiraishi, K., Ellis, D.J., Hiroi, Y., Fanning, C.M., Motoyoshi, Y., Nakai, Y., 1994. Cambrian orogenic belt in East Antarctica and Sri Lanka: implications for Gondwana assembly. Journal of Geology, 102, 47–65.
- Takahashi, K., Tsunogae, T., Santosh, M., Takamura, Y., Tsutsumi, Y., 2018. Paleoproterozoic (ca. 1.8 Ga) are magmatism in the Lützow-Holm Complex, East Antarctica: implications for crustal growth and terrane assembly in erstwhile Gondwana fragments. Journal of Asian Earth Science 157, 245–268.
- Takamura. Y., Tsunogae, T., Tsutsumi, Y., 2020. U–Pb geochronology and REE geochemistry of zircons in mafic granulites from the Lützow-Holm complex, East Antarctica: Implications for the timing and P–T path of post-peak exhumation and Antarctica–Sri Lanka correlation. Precambrian Research 348, 105850.
- Taylor, R., Clark, C., Fitzsimons, I. C. W., Santosh, M., Hand, M., Evans, M., Mcdonald, B., 2014. Post-peak, fluid-mediated modification of granulite facies zircon and monazite in the Trivandrum Block, southern India. Contributions to Mineralogy and Petrology 168, 1–17.

# Earthquake cycle in lower crust recorded in pseudotachylyte: insights from Mt. Sones and Mt. Riiser-Larsen, Napier Complex, East Antarctica

Ryo Murayama<sup>1</sup>, Lakshmanan Sreehari<sup>1</sup>, Tsuyoshi Toyoshima<sup>2</sup>

1, Shimane University
2, Niigata University

In Napier Complex, pseudotachylyte have been reported at four locations: Mt. Riiser-Larsen (e.g. Ishizuka et al., 1998), Mt. Sones (Toyoshima, JARE 60), Tonagh Island (Toyoshima et al., 1999) and McIntyre Island (Motoyoshi, 1996). At Tonagh Island, the various generations of pseudotachylyte formed during the deformation of UHT metamorphic rocks have been extensively studied, focusing on their distribution and microstructural characteristics, and it has been shown that there were repeated brittle failure and ductile deformation (Toyoshima et al., 1999). In contrast, pseudotachylyte found along Riiser-Larsen Main Shear Zone (RLMSZ) have been reported in several previous research (e.g. Ishizuka et al., 1998), but detailed structural and microstructural analyses remain limited. The same is true for pseudotachylytes from Mt. Sones The purpose of this study is to classify pseudotachylyte at Mt. Riiser-Larsen and Mt. Sones form microstructure and to clarify earthquake cycle in the Napier Complex.

In Mt. Sones, pseudotachylyte can be classified into three types based on field and microstructural observations.

Type A: This pseudotachylyte penetrates felsic gneiss and has sharp boundary with the host rock, injection vein, and chilled margin also present. The clasts in the vein are composed of quartz, plagioclase and pyroxene. Notably, garnet with cauliflower-like textures, likely crystallized from melt, is observed, with size increasing towards the center of the veins. Matrix of the veins is composed of acicular microlite of pyroxene. These garnet and pyroxene are often in mutual contact.

Type B: Pseudotachylyte with Round clasts: These brown pseudotachylytes penetrate felsic gneiss and have flow structure and injection vein. Rounded clasts of the veins are composed of fragments of recrystallized and cataclastic host rock and aligned in same direction.

Type C: This pseudotachylyte overprint undeformed dolerite. The clasts of the vein are composed of fragments of dolerite. In RLMSZ at Mt. Riiser-Larsen, pseudotachylyte can be classified into four types.

Type 1: Mylonitized pseudotachylyte: This pseudotachylyte is overprinted by ductile deformation. The host rock is mylonitic felsic gneiss that contains pyroxene porphyroclast with the edges altered to amphibole. The vein has sharp boundary with the host rock, and contains feldspar porphyroclast with homogeneous, fine-grained matrix.

Type 2: Pseudotachylyte with Angular Clasts: This pseudotachylyte penetrates orthogneiss and has sharp boundary with the host rock and chilled margin. Angular clasts of the vein are composed of fragments of recrystallized or cataclastic host rock and are randomly oriented with the matrix containing pyroxene microlite with acicular, dendritic, and spherulitic textures.

Type 3: Pseudotachylyte with Rounded Clasts: This pseudotachylyte intruded parallel to the boundary between different orthogneiss and have characteristics such as flow structure and injection vein. Rounded Clasts of the vein are composed of the fragment of recrystallized host rock and slightly aligned in same direction. Matrix of the vein have granular microlite of pyroxene, amphibole and ilmenite.

Type 4: This pseudotachylyte penetrates undeformed dolerite. The clasts of the vein are angular and are composed of fragments of dolerite host rock with granular microlite of pyroxene, plagioclase and ilmenite.

Above microstructure, Type 1 pseudotachylyte of RLMSZ indicates repetitive brittle failure and ductile deformation and Type A pseudotachylyte of Mt. Sones suggests a lower crustal origin. Furthermore, microstructure of Type B and C of Mt. Sones are consistent with that of Type 3 and 4 of RLMSZ. Although the types of pseudotachylyte in both regions are not completely consistent, both regions show seismicity from the upper to lower crust.

There are lower crustal shear zones such as Tonag Island (Toyoshima et al., 1999) and the RLMSZ (Murayama and Sreehari, under review), and lower crustal earthquakes have been reported in these areas. Microstructures from Tonagh Island, RLMSZ and Mt. Sones also points to lower crustal earthquake in all locations. These evidence points to the fact that there were some regional lower crustal shearing and lower crustal earthquake events in Napier Complex. Further details of these processes will be explored in future research.

#### Reference

Ishikawa, M., Hokada, T., Ishizuka, H., Murai, H., Suzuki, S., Takada, M. and Zartz, D. P. (2000). Geological map of Mount Riiser-Larsen, Enderby Land, Antarctica. Antarctic Geological Map Series Sheet 37. National Institute of Polar Research, Tokyo.

- Ishizuka, H., Ishikawa, M., Hokada, T. and Suzuki, S. (1998). Geology of the Mt. Riiser-Larsen area of the Napier Complex, Enderby Land, East Antarctica. National Institute of Polar Research Polar Geoscience, 11, 154–171.
- Motoyoshi, Y. (1996). Pseudotachylyte from McINTYRE Island, Enderby Land, East Antarctica: Evidence for a rapid crystallization. Proceedings of NIPR Symposium on Antarctic Geoscience, 9, 65–75.
- Toyoshima, T., Osanai, Y., Owada, M., Toshiaki, T., Hokada, T. and Crowe, W. A. (1999). Deformation of ultra-high temperature metamorphic rocks from Tonagh Island in the Napier Complex, East, Antarctica. Polar Geoscience, 12, 29–48.

### Timing of metamorphism at the Instekleppane, Lützow-Holm Complex, East Antarctica

Tatsuro ADACHI<sup>1</sup>, Lakshmanan SREEHARI<sup>2</sup>, Yuki MORI<sup>3</sup> and Tokokazu HOKADA<sup>4,5</sup>

<sup>1</sup>kyusyu University

<sup>2</sup>Shimane University

<sup>3</sup>University of Hyogo

<sup>4</sup>National Institute of Polar Research

<sup>5</sup>Graduate University for Advanced Studies (SOKENDAI)

Eastern part of the Dronning Maud Land including the Lützow-Holm Complex, East Antarctica is thought to have been situated in the collision zone between East and West Gondwana during the final stage of amalgamation of the Gondwana supercontinent (e.g., Stern, 1994). Several orogenies explaining the amalgamation of the Gondwana have been discussed: Jacobs and Thomas (2004) proposed East African–Antarctic Orogen (EAAO) which is one huge orogenic belt that was active for a long period (ca. 650–500 Ma), on the other hand, Meert (2003) proposed two crossing orogens where East African Orogen (EAO, Stern, 1994) being active during 750–620 Ma and Kuunga Orogen during 580–500 Ma, however there is no consensus about geological history of the orogenies so far.

The main tectonothermal event of the Lützow-Holm Complex was previously thought to have occurred around 550–530 Ma. However, a summary of U–Pb ages from this complex (Dunkley et al., 2020) suggests that ca. 600 Ma rocks are sporadically distributed in the southern part of the Soya Coast. In such context, the 65th Japan Antarctic Research Expedition (JARE65) conducted a geological survey one of its targets being to reveal the distribution of ca. 600 Ma metamorphic/igneous rocks in the LHC.

Instekleppane is an exposure approximately  $1.5 \text{ km} \times 2.0 \text{ km}$ , located in the southernmost part of the Lützow-Holm Bay, on the eastern shore of the Shirase Glacier. The common lithologies of this exposure are felsic Opx-Bt gneiss and leucocratic Grt-Bt gneiss with mafic to ultramafic Opx-Cpx-Hbl granulites, felsic Grt-Opx-Bt gneisses and Mg-Al rocks such as Grt-Crd-Bt gneiss and Spr-Crd-Bt gneiss intercalated as layer and lenses. Grt-bearing rocks are distinctive at the western and the southern parts of this exposure. Adachi et al. (2025) identified reaction textures in Mg-Al rocks from this exposure that reflect decompression under ultrahigh-temperature (UHT) conditions, including Opx + Sil  $\rightarrow$  Spr + Crd and Grt  $\rightarrow$  Opx + Spr + Crd.

In this study, zircon U–Pb dating was conducted on representative lithologies of metamorphic rocks from Instekleppane to constrain the timing of metamorphism and the formation of the protoliths. Analyzed samples are the Spr-Crd-Bt gneiss (TA2024012401A-m) and the granitic Bt gneiss that is interlayered with it (TA2024012401A-f), the felsic Opx-Bt gneiss (TA2024012501A and TA2024012703A), the felsic Grt-Opx-Bt gneiss (TA2024012604), and the Opx-Grt-Crd gneiss (TA2024012701A).

Each zircon grain in the samples contains a core with a distinct oscillatory zoning, and surrounding domains that overgrow the core, cutting across the oscillatory zoning and exhibiting vaguely zoned structures. These domains with vaguely zoned structure are interpreted to have formed during metamorphic processes. Based on cathodoluminescence (CL) brightness and chemical composition (Th/U ratio and chondrite normalized Yb/Gd (Ybn/Gdn) ratio), multiple growth stages can be identified within these metamorphic domains. Although the number of metamorphic domains varies among samples, they consistently yield ages ranging from 600 to 530 Ma, suggesting that the entire outcrop may have undergone metamorphism since around 600 Ma. The core domains consistently yield discordant ages forming trends between ~2700 Ma and ~2300 Ma, indicating that the protoliths of Instekleppane originated in the late Archean to early Proterozoic. This is comparable to the UHT metamorphic locality Rundvågshetta, and supports the extension of the Rundvågshetta Suite proposed by Dunkley et al. (2020) to include Instekleppane.

#### References

Adachi, T., Sreehari, L., Mori, Y. and Hokada, T., 2025, Polar Science, in press.

Dunkley, D.J., Hokada, T., Shiraishi, K., Hiroi, Y., Nogi, Y., and Motoyoshi, Y., 2020, Polar Science, 26, 100606. Jacobs, J., and Thomas, R.J., 2004 Geology, 32, 721–724.

Meert, J.G., 2003 Tectonophysics, 362, 1-40.

Stern, R.J., 1994, Annual Review of Earth and Planetary Sciences, 22, 319-351.

#### Evolution of the Archean crust in the Indian Ocean coastal sector of Antarctica

Tomokazu Hokada<sup>1,2</sup> and Simon L. Harley<sup>3</sup>

<sup>1</sup> National Institute of Polar Research, Tokyo 190-8518, Japan

<sup>2</sup> Polar Science Program, The Graduate University for Advanced Studies, SOKENDAI, Tokyo 190-8518, Japan

<sup>3</sup> School of Geosciences, University of Edinburgh, Edinburgh EH9 3FE, UK

The Antarctic continent has a long crustal history, from Eoarchean through Proterozoic to early Phanerozoic. This presentation summarizes the evolution of Archean crustal fragments in the coastal sector of the Indian Ocean in Antarctica (Dronning Maud Land, Enderby Land, Kemp Land, and MacRobertson Land). The Napier Complex, located in Enderby Land and western Kemp Land, is an ancient craton measuring 400 by 200 kilometers. It is characterized by fragments older than 3850 Ma and by high-temperature to ultrahigh-temperature regional metamorphism that occurred approximately 2550 to 2480 Ma. Thus, the Napier Complex records a crustal history spanning nearly the entire Archean period. Available data, though sparse relative to the large area covered, suggest that several crustal components of different ages came together to form the terrane. Numerous studies have focused on the UHT metamorphism of this terrane, which exhibits peak metamorphic temperatures of 1000-1100°C and subsequent isobaric cooling, along with some local variations in P-T evolution. In addition to the Napier Complex, the surrounding Proterozoic metamorphic terranes—such as the Lützow-Holm Complex, the Western Rayner Complex, the Rayner Complex, and the Rauer Islands—include several relatively small Archean crustal blocks. Some areas of the Rayner Complex are believed to be reworked parts of the Napier Complex, including the Oygarden Islands and the Edward VIII Gulf area. UHT metamorphism of Neoproterozoic-to-Cambrian age has also been demonstrated in these complex, polymetamorphic areas containing Archean protoliths (e.g., Rundvågshetta, Forefinger Point, and the Mather Supracrustals). Please see Hokada and Harley (2025) for details.

#### References

Hokada, T., Harley, S.L., Evolution of the Archean crust in the Indian Ocean coastal sector (Napier Complex, and nearby areas) of Antarctica – Review. Polar Science, in press, 2025. <a href="https://doi.org/10.1016/j.polar.2025.101266">https://doi.org/10.1016/j.polar.2025.101266</a>

# U-Pb geochronology with Th/U ratio in metamorphic zircon: example of felsic gneiss from Mt. McMaster, Napier Complex, East Antarctica

Mami Takehara<sup>1</sup>, Kenji Horie<sup>1,2</sup>, Tomokazu Hokada<sup>1,2</sup>, Allen Nutman<sup>3</sup>

<sup>1</sup>National Institute of Polar Research, Japan

<sup>2</sup>The Graduate University for Advanced Studies (SOKENDAI), Japan

<sup>3</sup>University of Wollongong, Australia

Thorium (Th) and uranium (U) are trace elements commonly used to evaluate the chemical environment during zircon crystallization, particularly through the Th/U ratio. Most igneous zircons from typical crustal rocks indicate Th/U ratios between 0.1 and 1. However, substitution mechanisms in zircon under natural conditions are more complicated (Rubatto, 2017, and references therein). It is widely accepted that Th/U ratios <0.1 in metamorphic zircons are influenced by the presence of Th-rich accessory phases (Yakymchuk et al., 2018, and references therein). Nevertheless, several previous studies reported that UHT metamorphic zircons (> 900°C) often display Th/U ratios > 0.1 and exhibit considerable variability, as summarized in Harley et al. (2007), Rubatto (2017), and references therein. To examine the thermal history of the nunataks outside of the ultra-high temperature metamorphism region in the Napier Complex, East Antarctica, we performed U-Th-Pb dating of zircon using a sensitive high-resolution ion microprobe at the National Institute of Polar Research on a felsic gneiss of Mt. McMaster. The zircons from the analyzed felsic gneiss sample yield apparent ages of 2462-2985 Ma, with the youngest peak at approximately 2484 Ma. Zircons with high Th/U ratios (>1) show a younger age peak centered at about 2475 Ma, whereas the zircons with low Th/U ratios (< 0.1) show an older peak centered at about 2486 Ma. This suggests two-stage zircon growth associated with regional metamorphism around 2.5 Ga. Additionally, premetamorphic zircons yield ages up to 2981 Ma, which is inconsistent with protolith ages of other felsic orthogneisses, matching that of a granitic gneiss from Mt. Riiser-Larsen.

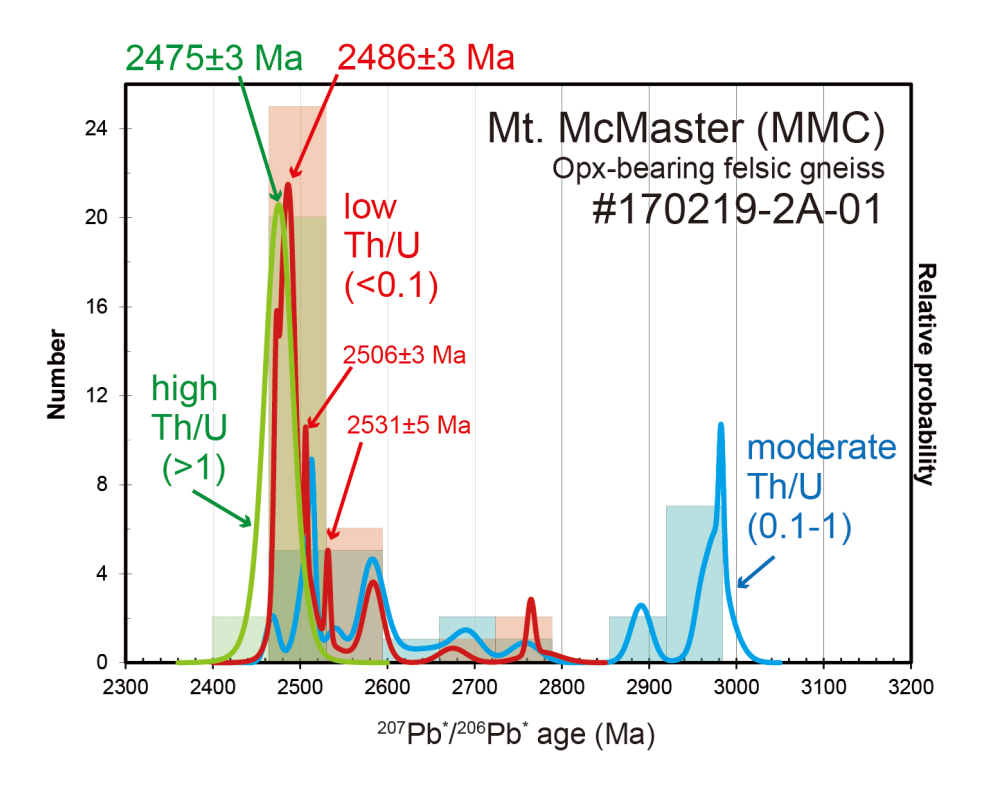


Figure 1. Probability density plots and histograms of  $^{207}\text{Pb}/^{206}\text{Pb}$  ages grouped based on the Th/U ratios in the MMC zircons (Takehara et al. under review). The three groups are shown in different colors. Green-colored ones have high Th/U ratios (>1), blue-colored ones have moderate Th/U ratios (0.1–1), and red-colored ones have low Th/U ratios (<0.1). The ages are calculated from the unmixing model.

## References

Harley et al. (2007) Elements, 3, 25-30. Rubatto (2017) Reviews in mineralogy and geochemistry, 83, 261-295. Yakymchuk et al. (2018) Journal of Metamorphic Geology, 36, 715-737. Takehara et al. Polar Science under review.

# Challenges in developing methods for integrating and complementing geochemical data from multiple microanalytical techniques

Keita Itano<sup>1</sup>, <u>Mami Takehara</u><sup>2</sup>, Akifumi Okuno<sup>3</sup>, and Masataka Aizawa<sup>4</sup>

<sup>1</sup>Akita University

<sup>2</sup>National Institute of Polar Research

<sup>3</sup>The Institute of Statistical Mathematics

<sup>4</sup>Hokkaido University of Education, Sapporo Campus

Chemical composition serves as fundamental information across various scientific and industrial disciplines, including earth science as well as archaeology, materials science, and medical care. Advances in measurement techniques now allow for the precise quantification of elemental abundances through diverse microanalytical methods, resulting in the accumulation of extensive compositional datasets. In polar geological research, chemical composition data of rocks and minerals are obtained by scanning electron microscopy (SEM), electron probe microanalysis (EPMA), laser ablation inductively coupled plasma mass spectrometry (LA-ICP-MS), and secondary ion mass spectrometry (SIMS), including a sensitive high-resolution ion microprobe (SHRIMP). However, the integration and meta-analysis of chemical composition data obtained through different measurement techniques are sometimes hindered by data deficiencies, arising from factors such as detection limits.

As an example of measurement techniques used in earth sciences and archaeology, handheld X-ray fluorescence (XRF) enables non-destructive measurement of valuable archaeological artifacts and rock samples in the field. Although it has begun to be applied more broadly, it cannot accurately determine the concentration of trace elements with low concentrations due to the detection limit. Moreover, SIMS and LA-ICP-MS are capable of detecting trace element concentrations, but the specific types of trace elements measured vary across laboratories and publications due to instrument-specific limitations and differing research objectives. When integrating such chemical composition data, missing values inevitably pose a significant challenge.

This project aims to revisit chemical composition data analysis and promote data-driven research by addressing two key aspects: (1) the development of statistically robust methods for data imputation and integration, and (2) the enhancement of data infrastructure through the promotion of data acquisition, which has been limited due to high costs. This presentation will provide a detailed overview of the project.

#### Zircon Th/U ratio revisited

Kenji Horie<sup>1,2</sup>, Mami Takehara<sup>1</sup> and Keita Itano<sup>3</sup>

<sup>1</sup>National Institute of Polar Research

<sup>2</sup>The Graduate University for Advanced Studies, SOKENDAI

<sup>3</sup>Akita University

Zircon has been the most widely utilized minerals for geochronological and geochemical studies, and its trace element composition provides valuable insights into the metamorphic and magmatic processes of the Earth's lithosphere. Abundance ratio of thorium (Th) and uranium (U) in zircons have long been used as geochemical criteria to distinguish between magmatic and metamorphic origins. In principle, the Th/U ratio in zircon is controlled by the crystal structure of zircon and the ionic radii of the respective elements. The zircon crystals preferentially incorporate U over Th because ionic radius of Zr ([VIII]Zr4+: 0.84 Å) is is closer to that of U ([VIII]U4+: 1.00 Å) than to that of Th ([VIII]Th4+: 1.05 Å), resulting in typical Th/U ratios of less than 1 (Ewing, 1999; Hoskin and Schaltegger, 2003). Most igneous zircons derived from typical continental crustal rocks exhibit Th/U ratios greater than 0.1 but still below 1 (e.g., Kohn and Kelly, 2017). On the other hand, in metamorphic settings, the generally lower Th/U ratios in zircon are attributed to the preferential incorporation of Th into minerals with high partition coefficients for Th, such as monazite, which reduces the relative abundance of Th available for zircon crystallization (e.g., Yakymchuk et al., 2018). This presentation introduces recent interpretation method of U–Pb zircon ages based on the Th/U ratios.

The one example features zircon collected from a felsic gneiss at Mount McMaster in the Napier Complex, East Antarctica, reported by Takehara et al. (2025). Zircons that constitute the c. 2500 Ma age peak, which is interpreted to reflect ultrahigh-temperature (UHT) metamorphism, show a wide range of Th/U ratios from 0.02 to 4.85. The peak for U-rich zircons with Th/U < 0.1 shows the age at c. 2486 Ma, whereas zircons with Th/U < 1 show a younger peak at c. 2475 Ma. The absence of Th-rich accessory minerals such as monazite in the rock sample, along with a ~10 Ma temporal transition from low-Th/U to high-Th/U zircon, makes it difficult to explain these observations using conventional models. It can be explained that the early-stage zircons grew in a relatively closed system during metamorphism, preferentially incorporating U. In the later stages, when Th-bearing minerals did not form and the relative abundance of Th increased, newly formed zircons incorporated more Th, resulting in elevated Th/U ratios. Previous studies have also reported that zircons subjected to UHT metamorphism exceeding 900 °C can display a wide range of Th/U ratios, often exceeding 0.1 (e.g., Harley et al., 2007; Rubatto, 2017; Bea et al., 1994).

#### References

Bea F, Pereira MD, Stroh A, Mineral/leucosome trace-element partitioning in a peraluminous migmatite (a laser ablation-ICP-MS study). Chemical Geology, 117, 291-312, 1994.

Ewing RC, Nuclear waste forms for actinides. Proceedings of the National Academy of Sciences, 96, 3432-3439, 1999.

Hoskin PWO, Schaltegger U, The composition of zircon and igneous and metamorphic petrogenesis. Reviews in mineralogy and geochemistry, 53, 27-62, 2003.

Kohn MJ, Kelly NM, Petrology and geochronology of metamorphic zircon. Microstructural geochronology: Planetary records down to atom scale, 35-61, 2018.

Harley SL, Kelly NM, Möller A, Zircon behaviour and the thermal histories of mountain chains. Elements, 3, 25-30, 2007.

Rubatto D, Zircon: The metamorphic mineral. Reviews in mineralogy and geochemistry, 83, 261-295, 2017. Takehara M, Horie K, Hokada T, Nutman AP, Zircon geochronology of Mt. McMaster and Aker Peaks, Napier Complex, East Antarctica. Polar Science, in-press.

Yakymchuk C, Kirkland CL, Clark C, Th/U ratios in metamorphic zircon. Journal of Metamorphic Geology, 36, 715-737, 2018.	

# Phase equilibrium modeling of multilayer corona textures around olivine in metagabbros from the Mozambique Belt in central Malawi

Mirei Kume, Toshiaki Tsunogae, Mzee Nkhwachi Nyirongo

University of Tsukuba

Corona textures are micro-scale textures within rocks that dominantly underwent rapid recrystallization of protoliths due to sudden changes in temperature and/or pressure (Torres-Rodriguez et al., 2021). Detailed petrographical and mineral chemical studies of the formation mechanisms of such corona textures are therefore crucial for evaluating metamorphic and/or cooling processes of the host rocks. In this study, we focus on an orthopyroxene-garnet-pargasite multilayer corona texture observed around olivine within metagabbros from the Neoproterozoic Mozambique Belt in central Malawi. The metagabbro occurs as small (1.1 x 1.5 km) and rounded to irregular bodies in the metasedimentary unit of the Malawi Basement Rocks. Tsunogae et al. (2021) estimated the peak metamorphism of the basement rocks in Lilongwe area as 9.1–11.6 kbar and 840 °C – 930 °C based on conventional geothermobarometry and phase equilibria modeling of metabasites, and the timing of the high-grade event as 569–557 Ma based on zircon geochronology. Geochemical characters of the metagabbros such as higher Th/Yb ratios in the Nb-Th-Yb diagram indicate their magmatic-arc origin. Although no age data has been obtained from the metagabbro, the decrease in grain size of plagioclase and clinopyroxene from the center toward the margin of the body in contact with the host gneisses (e.g., quartzite) suggest that the metagabbro probably intruded into the Malawi Basement Rocks during the Neoproterozoic high-grade metamorphism. In this study, we aim to infer the formation processes of this corona texture based on the microtextural analysis and chemical composition of the constituent minerals, as well as phase equilibrium modeling technique.

Microscopic observations revealed that the corona texture around olivine identified in the metagabbro is composed of four mineral layers, outward from the center: orthopyroxene, pargasite-1, garnet, and pargasite-2. Also, this corona texture is found only along the olivine-plagioclase boundaries, whereas no corona is formed around olivine in contact with other minerals. Therefore, this corona texture is considered to have formed through a reaction of olivine and plagioclase:

The results of hornblende-plagioclase geothermometry applied to a biotite-hornblende gneiss from the adjacent basement rocks showed a temperature range of 670–710 °C which is slightly lower than that of the peak P-T condition. As the crystallization temperature of olivine gabbro is inferred to be >1100 °C, the gabbro was probably cooled rapidly for more than 400 °C and formed the corona texture.

I order to quantitatively investigate the formation conditions of the corona texture, we constructed *P*–*X* pseudosections using olivine and plagioclase compositions as two end members, and evaluated the stability relations of the product minerals (garnet, orthopyroxene, and pargasite). In the pseudosections, garnet is abundant under high pressure conditions and also in the flelds close to the plagioclase end member. On the other hand, orthopyroxene is more stable at low pressure condition, but becomes more abundant in olivine-rich fields under high pressure. Although the modal abundance of pargasite does not show obvious differences depending on pressure and composition, its formation requires the presence of H<sub>2</sub>O. As our textural observations suggest that pargasite formed together with garnet and orthopyroxene, the intrusion of gabbro and local dehydration of the host basement rocks probably supplied H<sub>2</sub>O which probably contributed to the formation of this hydrous corona texture.

#### References

- Torres-Rodriguez, N., Barnes, S.J., Taranovic, V., Pearce, M.A., Verrall, M., Schoneveld, L.E., 2021. Reaction coronas at olivine–plagioclase contacts in host rocks from the Nova–Bollinger Ni–Cu–Co Deposit, Albany–Fraser Orogen, Western Australia: Evidence of a magmatic to metamorphic continuum. Journal of Petrology, 62, 1–24.
- Tsunogae, T., Uthup, S., Nyirongo, M.W., Takahashi, K., Rahman, Md.S., Liu, Q., Takamura, Y., Tsutsumi, T., 2021. Neoproterozoic crustal growth in Southern Malawi: New insights from petrology, geochemistry, and U–Pb zircon geochronology, and implications for the Kalahari Craton–Congo Craton amalgamation. Precambrian Research 352, Article 106007, p1-20.

## Neoarchean Th-U-total Pb monazite ages from the northern margin of the Kaapvaal Craton: New insights for understanding the evolution of the Limpopo Complex in southern Africa

Toshiaki Tsunogae<sup>1,2</sup> and Tatsuya Koizumi<sup>3</sup>

<sup>1</sup>Institute of Life and Environmental Sciences, University of Tsukuba, Ibaraki, Japan <sup>2</sup>Department of Geology, University of Johannesburg, Auckland Park, Republic of South Africa <sup>1</sup>Graduate School of Life and Environmental Sciences, University of Tsukuba, Ibaraki, Japan

The Limpopo Complex in southern Africa is an example of continental collision-type orogens formed by the assembly of Paleo- to Neoarchean cratons (the Zimbabwe Craton to the north and the Kaapvaal Craton to the south) during Neoarchean (e.g., van Reenen et al., 1992). Available geochronological data from the complex suggest that the collision took place at ca. 2.7–2.6 Ga, although ca. 2.0 Ga metamorphic ages have also been reported from the Central Zone (dominantly composed of granulite-facies to UHT metasediments) and the Northern Marginal Zone (NNZ, dominantly composed of charnockites and TTG gneisses with minor metabasites and meta-BIF) adjacent to the Zimbabwe Craton. Recently, such ca. 2.0 Ga thermal events are also reported from greenstone belts along the southern margin of the Zimbabwe Craton (Tsunogae and Belyanin, 2020; Kutsuzawa and Tsunogae, 2025). In contrast, no 2.0 Ga age has been obtained from the Southern Marginal Zone (SMZ) adjacent to the Kaapvaal Craton. In this study, we thus performed monazite Th-U-total Pb geochronology for metapelites from the northern margin of the Kaapvaal Craton, and evaluated the age differences with the Zimbabwe Craton margin. The analyzed metapelite samples were collected from two major greenstone belts in the northern margin of the Kaapvaal Craton; the Rhenosterkoppies Greenstone Belt and the Giyani Greenstone Belt. Both of them underwent amphibolite-facies metamorphism possibly related to the loading of the SMZ onto the Kaapvaal Craton during the Limpopo orogeny (Koizumi et al., 2023). The calculated ages are 2.81 Ga (Rhenosterkoppies) and 2.74 Ga (Giyani), which are almost equivalent to the age of the Zimbabwe Craton-Kaapvaal Craton collision and the metamorphism of the Limpopo Complex. No Paleoproterozoic age has been obtained. A recent tectonic model of the Limpopo Complex suggested Neoarchean double-sided subduction and following collision of the Zimbabwe and Kaapvaal Cratons (Tsunogae et al., 2025), and regarded both the NMZ and the SMZ as high-grade equivalents of the adjacent Zimbabwe and Kaapvaal Cratons, respectively. In contrast, the post-2.6 Ga crustal evolution of the two marginal zones and adjacent cratons are probably very different. Tsunogae et al. (2025) discussed that the heat source of such ca. 2.0 Ga event might be related to the activity of mantle plume underneath the Kalahari Craton, although this hypothesis must be evaluated by further geochronological investigation of the Limpopo Complex and adjacent cratons.

#### References

- Koizumi, T., Tsunogae, T., van Reenen, D.D., Smit, C.A., Belyanin, G.A., 2023. Fluid migration along deep crustal shear zone: A case study of the Rhenosterkoppies Greenstone Belt in the northern Kaapvaal Craton, South Africa. Geological Journal 58(10), 3928-3947.
- Kutsuzawa, Y., Tsunogae, T., 2025. Paleoproterozoic (ca. 2.0 Ga) monazite Th–U–total Pb ages from the Buhwa Greenstone Belt in the southern margin of the Archean Zimbabwe Craton: implications for Paleoproterozoic thermal overprinting. Abstract volume, the 16th Symposium on Polar Science, Tachikawa, Japan.
- Tsunogae, T., Belyanin, G.A., 2020. *P-T* and Ar-Ar age constraints on low- to high-grade metabasites from the Buhwa Greenstone Belt, southern Africa: Implications for Neoarchean to Paleoproterozoic thermal evolution along the Limpopo Complex-Zimbabwe Craton boundary. Journal of African Earth Sciences, 162, Article 103722, 1-17.
- Tsunogae, T., Rahman, Md.S., Gao, P., Santosh, M., Fujisaki, W., Uthup, S., Mandingaisa, P., 2025. Neoarchean arc magmatism and crust recycling in the Northern Marginal Zone of the Limpopo Complex, Zimbabwe: New insights from zircon U-Pb-Hf isotopes of a charnockite suite. Geological Journal, doi:10.1002/gi.5248.
- van Reenen, D.D., Barton, J.M., Jr., Roering, C., Smit, C.A., van Schalkwyk, J.F., 1987. Deep crustal response to continental collision: The Limpopo belt of southern Africa. Geology, 15, 11-14.

# Paleoproterozoic (ca. 2.0 Ga) monazite Th-U-total Pb ages from the Buhwa Greenstone Belt in the southern margin of the Archean Zimbabwe Craton: implications for Paleoproterozoic thermal overprinting

Yoko Kutsuzawa¹ and Toshiaki Tsunogae²
¹ College of Geosciences, University of Tsukuba, Japan
² Institute of Life and Environmental Sciences, University of Tsukuba, Japan

Available petrological and geochronological data from various cratons and orogenic belts in southern Africa suggest that the collision of the Zimbabwe Craton (ZC) and the Kaapvaal Craton (KC), and the formation of the Limpopo Complex (LC) (suture zone) took place during Neoarchean (ca. 2.7–2.6 Ga; van Reenen et al., 1987) possibly related to the amalgamation of the Kenorland supercontinent. Although slightly younger (ca. 2.0 Ga) ages have also been reported from the LC (e.g., Kamber et al., 1995), they are dominantly from shear zones (e.g., Triangle Shear Zone) and been considered as an event of post-collisional crustal reworking. However, recent geochronological studies reported similar ca. 2.0 Ga events from other parts of the LC and also from the Buhwa Greenstone Belt (BGB) in the southern margin of the ZC adjacent to the LC (Tsunogae and Belyanin, 2020). Therefore, detailed geochronological investigations are necessary to be done from the region to better understand the evolution of this collisional orogen. We thus conducted monazite Th–U–total Pb dating for various lithologies from the BGB using EPMA.

The ZC consists of TTG gneisses (ca. 3.5 to 2.8 Ga felsic to mafic orthogneisses), greenstone belts (metamorphosed basalt and komatiite lavas (ca. 3.2 to 2.7 Ga) with metasediments), and intrusive granites (2.9 to 2.6 Ga) as well as 2.58 Ga ultramafic-mafic intrusion of the Great Dyke (Wilson et al., 1995). The BGB, which is the focus of this study, occurs as an ENE-WSW-trending linear zone along the southern margin of the ZC. It is distributed parallel to the boundary between the ZC and the LC, approximately 1 to 5 km north from the ZC–LC boundary. Tsunogae and Belyanin (2020) reported, based on the increase of metamorphic grade from epidote-amphibolite facies to amphibolite facies toward the ZC–LC contact, that the BGB was thermal recrystallized due to the effect of loading of the "hot" high-grade LC onto the "cold" low-grade ZC due to a "hot-iron effect" during the compression event related to the ca. 2.7–2.6 Ga ZC–KC collision.

The BGB is composed of metasedimentary and metavolcanic rocks including metamorphosed sandstones, shales, cherts, BIF, limestones, and basalts (Worst, 1962). Fedo and Eriksson (1996) reported detrital zircon ages of 3.25–3.09 Ga from the sedimentary protoliths of these rocks. Younger granitoid intrusions are also characteristic around the BGB: the 2.67–2.5 Ga Razi Granite and the 2.7–2.6 Ga Chibi Granite which have been regarded as syn- to post-tectonic intrusions. Recently, Tsunogae and Belyanin (2020) obtained amphibole Ar-Ar ages of ca. 2.53 Ga and ca. 2.02–1.97 Ga from three metabasite samples of the BGB.

So far, we examined 28 thin sections from the BGB, and obtained reliable ages from three metasediment (muscovite-quartz schist) samples; ca. 2.8 Ga from sample BH1-1 (from the northernmost part of the eastern BGB), ca. 2.7 Ga and 2.0 Ga from sample BH1-23B (from the southern part of the eastern BGB near the LC), and 2.0 Ga from sample BH2-11B (from the central BGB).

The 2.7–2.8 Ga ages are consistent with the timing of the ZC–KC collision, whereas the samples from the southern BGB near the ZC–LC boundary record younger metamorphic ages of ca. 2.0 Ga. Since previous studies reported a 2.0 Ga thermal event from the southern BGB (Tsunogae and Belyanin, 2020), it is reasonable to infer that the distinct thermal event occurred at ca. 2.0 Ga along the ZC–LC contact zone.

The implication of the ca. 2.0 Ga age is probably significant in the context of Paleoproterozoic crustal evolution, as the event coincided with the timing of the assembly of the supercontinent Columbia and also to the

intrusion of the Bushveld Complex (ca. 2.06 Ga) in the northern KC. Therefore, this period likely represents a stage of active continental reorganization possibly accompanied by large-scale heat input in the region, which probably gave rise to thermal overprinting in this region.

#### References

- Fedo, C.M., Erikkson, K.A. (1996) Stratigraphic framework of the ~3.0 Ga Buhwa Greenstone Belt: a unique stable-shelf succession in the Zimbabwe Archean Craton, Precambrian Research, 77, 161-178.
- Kamber, B.S., Kramers, J.D., Napier, R., Cliff, R.A., Rollinson, H. R. (1995) The Triangle Shearzone, Zimbabwe, revisited: new data document an important event at 2.0 Ga in the Limpopo Belt. Precambrian Research, 70, 191–213.
- Mkweli, S., Kamber, B., Berger, M. (1995) Westward continuation of the craton-Limpopo Belt tectonic break in Zimbabwe and new age constrains on the timing of the thrusting. Journal of the Geological Society, London, 152, 77-83
- Tsunogae, T., Belyanin, G.A. (2020) P–T and Ar–Ar age constraints on low- to high-grade metabasites from the Buhwa Greenstone Belt, southern Africa: Implications for Neoarchean to Paleoproterozoic thermal evolution along the Limpopo Complex–Zimbabwe Craton boundary. Journal of African Earth Sciences, 162, 103722
- van Reenen, D.D., Barton Jr., J.M., Roering, C., Smit, C.A., van Schalkwyk, J.F. (1987) Deep crustal response to continental collision: the Limpopo belt of southern Africa. Geology, 15, 11–14.
- Wilson, J.F., Nesbitt, R.W., Fanning, C.M. (1995) Zircon geochronology of Archaean felsic sequences in the Zimbabwe craton: a revision of greenstone stratigraphy and a model for crustal growth. Geological Society Special Publications, 95, 109–126.
- Worst, B.G. (1962) The geology of the Buhwa iron ore deposits and adjoining country: Belingwe district. South Rhodesia Geological Survey Bulletin, 53, 114pp.

# Monazite Th-U-total Pb geochronology of metasediments from the Abukuma Mountains, NE Japan: Preliminary report

Arisa Suwa<sup>1</sup> and Toshiaki Tsunogae<sup>2,3</sup>

<sup>1</sup>Degree Program in Geosciences, University of Tsukuba, Ibaraki, Japan

<sup>2</sup> Institute of Life and Environmental Sciences, University of Tsukuba, Ibaraki, Japan

<sup>3</sup>Department of Geology, University of Johannesburg, Auckland Park, Republic of South Africa

The Abukuma Mountains, located in northeast Japan between the Tanakura Tectonic Line and the Futaba Fault, is predominantly composed of Cretaceous plutonic rocks (granites, diorites, and gabbros) with minor metamorphic rocks such as the Abukuma metamorphic rocks in the central part, Hitachi and Nishidohira-Tamadare metamorphic rocks in southwestern part, Yamagami-Matsugadaira metamorphic rocks in the northeastern part, and Marumori metamorphic rocks in the northern part of the mountains. Numerous geochronological studies have been done for the plutonic rocks (e.g., Kubo and Yamamoto, 1990; Ishihara and Orihashi, 2015; Wang et al., 2023) and suggested a major age cluster from 126 to 96 Ma (Early to Late Cretaceous) with a minor magmatic event at 308-302 Ma (Carboniferous) obtained from the Wariyama Sheared Granodiorite in the northern part (Tsuchiya et al., 2014). In contrast, previous geochronological studies of the metamorphic rocks are limited, and reported only from the Abukuma, Nishidohira, and Yamagami metamorphic rocks (e.g. Hiroi et al., 1998; Yoneguchi et al., 2021; Miyashita et al., 2010; Otsuka and Tsunogae, 2024). The metamorphic ages from the Abukuma Mountains identified two major tectonic events: (1)  $^{206}\text{Pb}/^{238}\text{U}$  zircon ages of  $121.9 \pm 1.6$  Ma and  $111.9 \pm 2.3$  Ma from the Abukuma metamorphic rocks (Hiroi et al., 1998) and CHIME monazite age of 139 ± 24 Ma from the Nishidohira metamorphic rocks (Yoneguchi et al., 2021), (2) Late Devonian-Early Carboniferous K-Ar age of 322-287 Ma (Miyashita et al., 2010) and monazite Th-U-total Pb ages of  $333 \pm 46$  Ma and  $362 \pm 55$  Ma (Otsuka and Tsunogae, 2024) from the Yamagami metamorphic rocks. However, no systematic correlation of metamorphic ages in the Abukuma Mountains has been done do far. Constraining the timing of regional metamorphism through different geochronological methods is essential for reconstructing the Devonian to Cretaceous tectonic history of the Abukuma Mountains.

In this study, we conducted monazite Th-U-total Pb dating using Electron Probe Micro Analyzer (EPMA) to investigate metamorphic ages of discrete metasedimentary units throughout the Abukuma Mountains. Pelitic schist samples from the Marumori metamorphic rocks, Yamagami metamorphic rocks (Aoba area), and Nishidohira metamorphic rocks were analyzed. We obtained Th-U-total Pb monazite ages from the Marumori, Yamagami (Aoba area), and Abukuma metamorphic rocks as ca. 104 Ma, ca. 107 Ma, and ca. 111–104 Ma, respectively. The obtained ages cluster around 110–100 Ma which is almost equivalent to the published zircon ages of adjacent granitoid bodies, suggesting that the Cretaceous magmatic activity significantly influenced the study area. The above results imply that a contact metamorphism associated with the intrusion of Early Cretaceous (ca. 110–100 Ma) granitoids significantly recrystallized the pelitic shists of the study area, and partly overprinted the older metamorphic event.

#### References

Hiroi Y, Kishi S, Nohara T, Sato K, Goto J, Cretaceous high-temperature rapid loading and unloading in the Abukuma metamorphic terrane, Japan. J. Metamorphic Geol, 16, 67–81, 1998.

Ishihara S, Orihashi Y, Cretaceous granitoids and their zircon U–Pb ages across the south-central part of the Abukuma Highland, Japan. Island Arc, 24, 159–168, 2015.

Kubo K, Yamamoto T, Cretaceous intrusive rocks of the Haramachi district, eastern margin of the Abukuma Mountains – petrography and K-Ar age – . Jour. Geol. Soc. Japan, 96-9, 731–743, 1990.

Miyashita A, Yagi K, Itaya T, Phengite K–Ar ages of the Yamagami Metamorphic Rocks in the Motai-Matsugataira Belt – Probability of the extension of the Renge Metamorphic Belt to the Northeastern Japan Arc – . J. Geol. Soc. Japan, 126-2, 85–93, 2020.

- Otsuka Y, Tsunogae T, Monazite Th–U–total Pb geochronology of pelitic schists from the Yamagami metamorphic rocks in eastern Abukuma Mountains, NE Japan: Implications for Late Devonian Early Carboniferous high P/T metamorphism. Earth Evolution Sciences, 18, 2–8, 2024.
- Tsuchiya N, Takeda T, Tani K, Adachi T, Nakano N, Osanai Y, Kimura J, Zircon U–Pb age and its geological significance of late Carboniferous and Early Cretaceous adakitic granites from eastern margin of the Abukuma Mountains, Japan. The Journal of the Geological Society of Japan, 120–2, 37–51, 2014.
- Wang JY, Tsunogae T, Santosh M, Arc building in the Abukuma Mountains of NE Japan: Insights from petrology, geochemistry and zircon U-Pb-Hf isotope data. Lithos, 456–457, 107315, 2023.
- Yoneguchi Y, Tsunogae T, Takahashi K, Sakuwaha KG, Ikehata K, Pressure-temperature evolution of andalusite-kyanite-sillimanite-bearing pelitic schists from Nishidohira, southern Abukuma Mountains, Northeast Japan: Implications for Cretaceous rapid burial and exhumation in the Northeast Asian continental margin. Lithos, 406 –407, 106522, 2021.

# Paleomagnetic information from Proterozoic dikes in the Mt. Riiser-Larsen area of the Napier Complex, East Antarctica

Naoto Ishikawa<sup>1</sup>, Yoshimitsu Suda<sup>2</sup> and Shin-ichi Kagashima<sup>3</sup>

Department of Earth System Sciences, School of Sustainable Design, University of Toyama

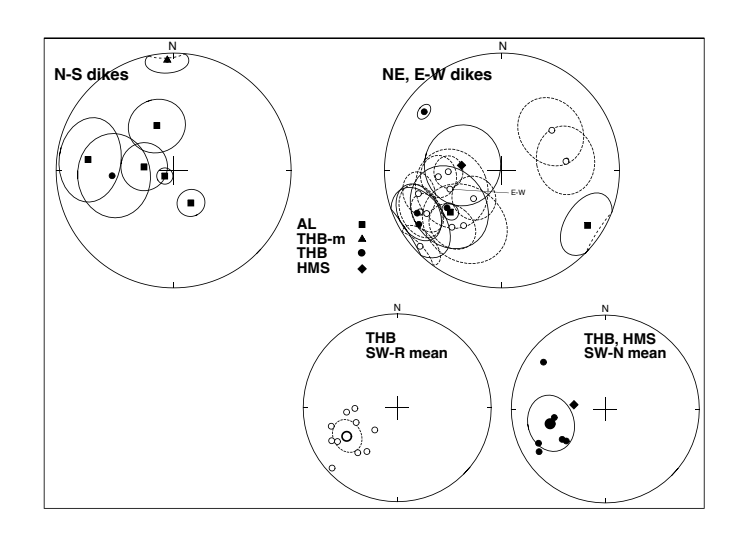
<sup>2</sup>Fucalty of Education, Nagasaki University

<sup>3</sup>Fucalty of Science, Yamagata University

Before the formation of the Gondwana continent, the Achean Napier complex and its surrounding areas in Enderby Land, East Antarctica, has been considered to have belonged to the India Craton (e.g., Boger, 2011). In oder to clarify tectonic movements in East Antarctica during the formation history of suppercontinents, paleomagnetic analyses have been performed on Proterozoic dikes intruding to the Napier Complex in the Mt. Riiser-Larsen area (RL). In the RL, there are many dikes, mainly striking N-S and NE-SW (Ishizuka et al., 1998). Suzuki et al. (2008) provided geochemical analyzed results from 15 dikes and classified the dikes into four types: tholeiite basalt (THB) and high-magnesian andesite (HMA) for NE-SW-striking dikes, and alkaline basalt (AL) and tholeiite basalt (THB-m) for N-S striking dikes. Suzuki et al. (2008) suggested that the Rb-Sr and Sm-Nd isotope data for the THB and the AL dykes defined 2.0-1.9 Ga and 1.2 Ga, respectively. Samples of the dikes in this study were collected at 3sites in JARE 35 and 53 sites in JARE 46, including the dikes analyzed by Suzuki et al. (2008): N-S striking dikes (N-S dikes) at 16 sites, NE-SW-striking dikes (NE dikes) at 36 sites and E-W-striking (E-W dikes) at 4 sites. XRF analyses for measuring whole-rock chemical compositions were performed on samples from 46 sites. By using geochemical data of this study and Suzuki et al. (2008), dikes of 54 sites were divided as follows: N-S dikes of AL at 5 sites, THB-m at 5 sites, THB at 2 sites and HMA at 1 site; NE dikes of AL at 1 site, THB-m at 2 sites, THB at 30 sites and HMA at 4 sites; E-W dikes of THB at 3 sites.

Progressive thermal and alternating-field demagnetization experiments provided the stable magnetic components carried by magnetite, which were isolated at higher demagnetization steps generally between 500 and 550°C and/or between 15 and 30 mT. Directions of the components were estimated by applying the principal component analysis to liner trends of the demagnetization curves decaying toward the origin of the vector end point diagram. Estimated directions with maximum angular deviation of 10° or less were used for the further consideration. Site mean directions of the components with radius of 95% confidence circle (alpha-95) smaller than 30° were obtained from the following 26 sites (Figure 1): 7 sites of the N-S dikes (AL: 5 sites, THB-m: 1 site, THB: 1 site) dikes, 18 sites of the NE dikes, (AL: 2 sites, THB 15 sites, HMA: 1 site), and 1 site of the E-W dike (THB). Directions of the N-S dikes with positive inclination are scattered, although the directions, except for the THMm dike, appear to be roughly grouped with westward declination. Directions of the NE-THB dikes are divided mainly into the following three types: (1) directions with southwestward declination and positive inclination (SW-N), (2) those with northeastward declination and negative inclination (NE-R), and (3) those with southwestward declination and negative inclination (SW-R). The NE-R directions are antipodal to the SW-R ones. A direction of the HMA dikes is close to the SW-R directions. One of the two AL dikes is close to the SW-R ones, while the other is different from the directions of the three types. A direction of the E-W dike is similar with the SW-R ones. A mean calculated from the SW-N and reversed NE-R directions including that of the HMA dike is D =254.9°, I = 28.5° and alpha-95 = 22.3° (SW-N mean). A mean of the SW-R directions including that of the E-W dike is D = 240.5°, I = -38.4° and alpha-95 = 13.3° (SW-R mean). The SW-N and SW-R means are considered to be the characteristic directions of the Proterozoic dikes in the RL.

Virtual geomagnetic poles (VGPs) of the N-S striking AL dikes and mean VGPs of the SW-R and SW-N means are shown in Figure 2. Paleomagnetic poles of 0.55-2.4 Ga from the India Craton are also plotted in the Gondwana frame as shown in Figure 2 (Torsvik and Van der Voo, 2002; Gregory et al., 2006; Li et al., 2008; Malone et al., 2008; Gregory et al., 2009; Pradhan et al., 2012., Belica et al., 2014; Nagaraju et al. 2018; Ramesh et al. 2018; Shankar et al., 2018; Parashuramula et al., 2023). The VGPs of the N-S striking AL dikes are scatted, but the four of the VGPs appear to be located around 1.0-1.2 Ga poles of India. The mean VGP of the SW-R is close to the 2.18 Ga poles, while that of the SW-N seems not to be fitted with the Proterozoic paleopoles of India in the Gondwana frame. The mean VGPs of the SW-R and SW-N may imply that the Napier complex may have been located at low latitude.



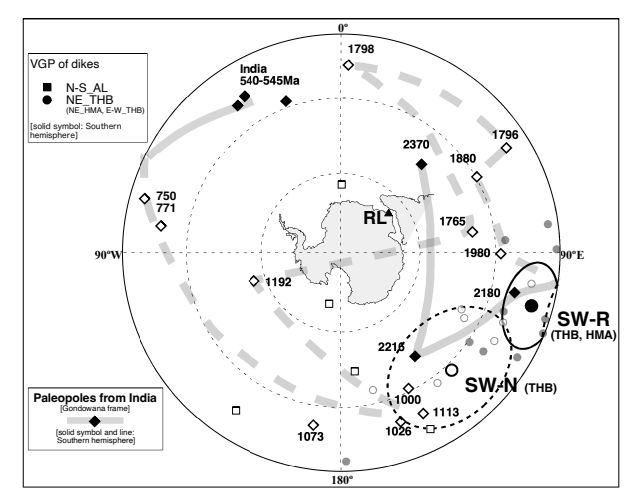


Figure 1. Site means of the stable magnetic components from Proterozoic dikes in the Mt. Riiser-Larsen area (RL).

Figure 2. Positions of VGPs from the dikes in the RL and 0.5-2.4 Ga paleomagnetic poles from the India Craton.

#### References

Belica, M.E., Piispa, E.J., Meert, J.G. et al., Paleoproterozoic mafic dyke swarms from the Dharwar Craton; paleomagnetic poles for India from 2.37-1.88 Ga and rethinking the Columbia supercontinent. Precamb. Res., 244, 100–122, 2014.

Boger, S.D., Antarctica - Before and after Gondwana, Gondwana Research, 19, 335-371, 2011.

Gregory, L.C., Meert, J.G., Pradhan, V. et al., A paleomagnetic and geochronological study of the Majhgawan Kimberlite, India: implications for the age of the Vindhyan SuperGroup. Precamb. Res., 149, 65–75, 2006

Ishizuka, H, Ishikawa, M., Hokada, T. et al., Geology of the Mt. Riser-Larsen area of the Napier Complex, Enderby Land, East Antarctica, Polar Geoscience, 11, 154-171.

Li, Z.X., Bogdanova, S.V., Collins, A.S. et al., Assembly, configuration, and break-up history of Rodinia: A synthesis. Precamb. Res., 160, 179–210, 2008.

Malone, S.J., Meert, J.G., Banerjee, D.M. et al, Paleomagnetism and Detrital Zircon Geochronology of the Upper Vindhyan Sequence, Son Valley and Rajasthan, India: A ca. 1000 Ma Closure age for the Purana Basins? Precamb. Res., doi:10.1016/j.precamres.2008.04.004, 2008.

Nagaraju, E., Parashuramulu, V., Kumar, A. et al., Paleomagnetism and geochronological studies on a 450 km long 2216 Ma, dyke from the Dharwar craton, southern India, Phys. Earth and Planet. Interiors 274, 222–231, 2018.

Parashuramulu, V., Nagaraju, E., Shankar, R. et al., Paleogeography of India at ~1.8 Ga: New constraints from baddeleyite geochronology and paleomagnetism of mafic dykes from the Dharwar craton, Precamb. Res., 395, https://doi.org/10.1016/j.precamres.2023.107146, 2023.

Pradhan, V.R., Meert, J.G., Panditb, M.J. et al., Paleomagnetic and geochronological studies of the mafic dyke swarms of Bundelkhand craton, central India: Implications for the tectonic evolution and paleogeographic reconstructions, Precamb. Res., 198-199, 51-76, 2012.

Ramesh Babu, N., Venkateshwarlu, M., Shankar, R. et al., New paleomagnetic results on ~2367 Ma Dharwar giant dyke swarm, Dharwar craton, southern India: implications for Paleoproterozoic continental reconstruction, J. Earth Syst. Sci., 127, 3, https://doi.org/10.1007/s12040-017-0910-3, 2018.

Shankar, R., Srinivasa Sarma, D., Ramesh Babub, N. et al., Paleomagnetic study of 1765 Ma dyke swarm from the Singhbhum Craton: Implications to the paleogeography of India, J. Asian Earth Sciences, 157, 235–244, 2018.

Suzuki, S., Ishizuka, H. and Kagami, H., Early to middle Proterozoic dykes in the Mt. Riser- Larsen area of the Napier Complex, East Antarctica: tectonic implications as deduced from geochemical studies, in Satish-Kumar et al., (eds) Geodynamic Evolution of East Antarctica: A Key to the East-West Gondwana Connection. Geological Society, London, Special Publications, 308, 195-210. DOI: 10.1144/SP.308.10, 2008.

Torsvik, T. H., Van der Voo, R., Refining Gondwana and Pangea paleogeography: Estimates of Phanerozoic non-dipole (octupole) fields, Geophys. J. Int., 151, 771 – 794, doi:10.1046/j.1365-246X.2002.01799.x., 2002.

### Holocene Ice-Sheet Retreat history in Lützow-Holm Bay, East Antarctica

Yusuke Suganuma<sup>1,2</sup>, Kazuya Kusahara<sup>3</sup>, Moto Kawamata<sup>1,4</sup>, Takeshige Ishiwa<sup>1,2</sup>, Kota Katsuki<sup>5</sup>, Hiroto Kajita<sup>1,6</sup>, Shun Tsutaki<sup>1,2</sup>, Takashi Obase<sup>3</sup>, Motohiro Hirabayashi<sup>1</sup>, Masakazu Fujii<sup>1,2</sup>, Jun'ichi Okuno<sup>1,2</sup>

<sup>1</sup>National Institute of Polar Research, <sup>2</sup>The Graduate University for Advanced Studies (SOKENDAI), <sup>3</sup>JAMSTEC, <sup>4</sup>Civil Engineering Research Institute for Cold Region, <sup>5</sup>Shimane Univ. and <sup>6</sup>Hirosaki Univ.

Recent observations and model simulations highlight the role of warm Circumpolar Deep Water (CDW) in driving rapid ice-shelf thinning and increased ice discharge from the West Antarctic Ice Sheet, contributing to ongoing sealevel rise. While this mechanism is well established in West Antarctica and linked to post–Last Glacial Maximum deglaciation, its influence on East Antarctic ice-sheet dynamics remains less clear. Here, we reconstruct a detailed deglaciation history of Lützow-Holm Bay, East Antarctica, based on comprehensive geomorphological mapping and surface exposure dating (Be-10 and C-14) of glacial erratics and bedrock. Our results reveal that ice-sheet retreat initiated in the southeastern part of the bay along the Shirase submarine valley between ~9 and 5 ka, subsequently progressing northeastward between ~8 and 4 ka. High-resolution oceanographic modeling indicates that present-day elevated ocean temperatures in the southeastern bay are caused by CDW inflow through the submarine valley. We propose that this oceanographic configuration, combined with bathymetric focusing, promoted an asymmetric pattern of ice retreat during the early to mid-Holocene. These findings underscore the potential vulnerability of East Antarctic outlet glaciers to ocean warming and provide critical constraints for future ice-sheet and sea-level projections.

# Past and Present Environmental Conditions in the Larsemann Hills, East Antarctica: Evidence from Sediment Cores and Water Column Profiles

<u>Kotoha Kosugi<sup>1</sup></u>, Takeshige Ishiwa<sup>1,2</sup>, Mahesh Badnal<sup>3</sup>, Elie Verleyen<sup>4</sup>, Toru Tamura<sup>5</sup>, Cheryl Noronha-D'Mello<sup>3</sup>, Philippe Huybrechts<sup>6</sup>, Anish Kumar Warrier<sup>7</sup>, Kota Katsuki<sup>8</sup>, Minoru Ikehara<sup>9</sup>, Rahul Mohan<sup>3</sup>,

### Yusuke Suganuma<sup>1,2</sup>

<sup>1</sup>The Graduate University for Advanced Studies, <sup>2</sup>National Institute of Polar Research, <sup>3</sup>National Centre for Polar and Ocean Research, <sup>4</sup>Ghent University, <sup>5</sup>National Institute of Advanced Industrial Science and Technology, <sup>6</sup>Vrije Universiteit Brussel, <sup>7</sup>Manipal Academy of Higher Education, <sup>8</sup>Shimane University, <sup>9</sup>Kochi University

In recent years, parts of Antarctica have been significantly influenced by global climate change, with the accelerated melting of the ice sheet contributing to global sea-level rise. To better predict future climate change and their effects in Antarctica, coastal lake sediments are valuable archives, as they preserve high-resolution, longterm records of past changes in terrestrial and lacustrine environments. The Last Interglacial period (LIG; ~ 126,000 years ago) was warmer than the present one, and global mean sea level was ~ 6-9 meters higher than today (Dutton et al., 2015). However, terrestrial records from this period are scarce in Antarctica because many were eroded during the Last Glacial Maximum (LGM). In contrast, parts of the Larsemann Hills, East Antarctica, are believed to have reminded ice-free prior to and during the LGM (Hodgson et al., 2001), indicating that lake sediments in this region may contain continuous paleoenvironmental records extending back to the LIG. Previous studies have reported sedimentary sequences from this region including records from Kirisjes Pond, which extend into MIS3 (~ 50,000 years ago; Verleyen et al., 2004). Moreover, sea-level fluctuations and ice sheet changes along the East Antarctic coast have been reconstructed through stratigraphic and microfossil analyses (e.g., Hodgson et al., 2001; Verleyen et al., 2004). Nevertheless, further direct dating to the LIG sediments and highresolution analyses (on a decadal scale) potentially help to refine the understanding of paleoenvironmental changes since the LIG with various timescales. During the Antarctic expedition in 2024, with the aim of reconstructing the paleoenvironmental changes since the LIG, sediment cores were collected from 17 lakes in the Larsemann Hills. In addition, water column profiles (CTD data) were obtained to characterize the modern limnological and hydrological conditions of these lakes, which are crucial for understanding modern-day processes and linking them to the sedimentary record. Here, we present CTD profiles and preliminary results of a sediment core from Kirisjes Most coastal lakes in East Antarctica exhibit seasonal vertical changes in their water column resulting from ice cover in winter and ice melt in summer. Our CTD data suggest that Kirisjes Pond is a low-salinity lake and that the bottom-water circulation strongly influenced by salinity stratification in early summer. We compare these characteristics of the Larsemann Hills lakes in the early summer with data from other seasons (Noronha-D'Mello et al., 2023). For the sediment cores, lithological descriptions, X-ray CT imaging, and non-destructive analyses were conducted to identify stratigraphic features. Based on these results, we will discuss preliminary evidence of paleoenvironmental changes in Kirisjes Pond. Future work will include radiocarbon dating, OSL dating, and diatom assemblage analysis, integrated with lithological and CT analyses, to develop a comprehensive reconstruction of paleoenvironmental changes since the LIG in Kirisjes Pond and other lakes in the Larsemann Hills.

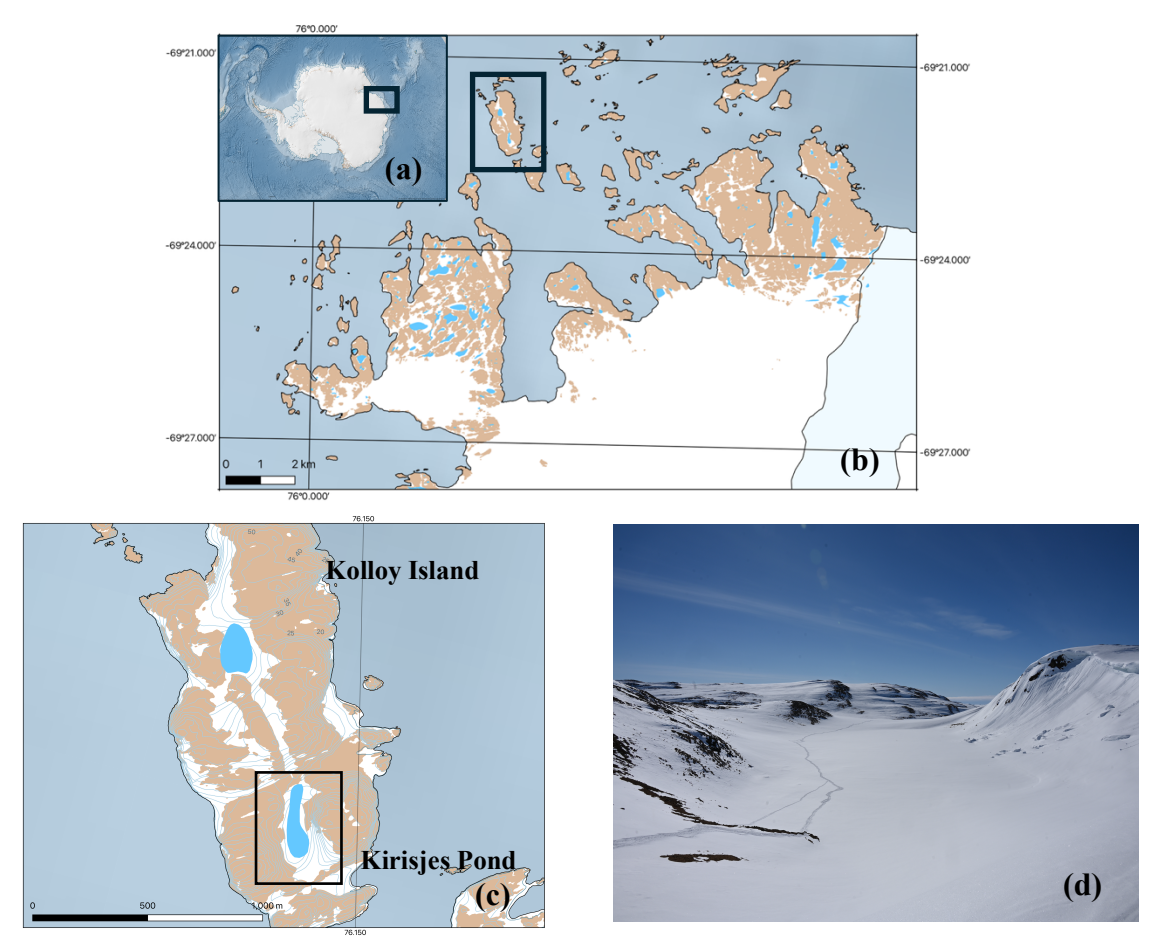


Figure 1: Location of the Larsemann Hills in East Antarctica (a). Kirisjes Pond located at Kolloy Island (the area indicated by the square) in the Laesemann Hills (b). Location of Kirisjes Pond in Kolloy Island (c) and photo (d). These maps were created using QGIS (<a href="https://www.qgis.org/">https://www.qgis.org/</a>) with data from Quantarctica

#### References

A. Dutton, A. E. Carlson, A. J. Long, G. A. Milne, P. U. Clark, R. DeConto, B. P. Horton, S. Rahmstorf, M. E. Raymo, Sea-level rise due to polar ice-sheet mass loss during past warm periods. Science, 349, aaa4019, 2015.

Elie Verleyen, Dominic A. Hodgson, Koen Sabbe and Wim Vyverman, Late Quaternary deglaciation and climate history of the Larsemann Hills (East Antarctica). Journal of Quaternary Science, 19, 361-375, 2004.

D. A. Hodgson, P. E. Noon, W. Vyverman, C. L. Bryant, D. B. Gore, P. Appleby, M. Gilmour, E. Verleyen, K. Sabbe, V. J. Jones, J. C. Ellis-Evans, P. B. Wood, Were the Larsemann Hills ice-free through the Last Glacial Maximum? Antarctic Science, 13, 440-454, 2001.

Cheryl A. Noronha-D'Mello, B. S. Mahesh, Jenson George, Shramik Patil, Avirajsinh Jadav, Rahul Mohan, Highresolution insights of physical properties of water columns of lakes at the Larsemann Hills, East Antarctica. Polar Science, 38, 1-10, 2023.

Kenichi Matsuoka, Anders Skoglund, George Roth, Jean de Pomereu, Huw Griffiths, Robert Headland, Brad Herried, Katsuro Katsumata, Anne Le Brocq, Kathy Licht, Fraser Morgan, Peter D. Neff, Catherine Ritz, Mirko Scheinert, Takeshi Tamura, Anton Van de Putte, Michiel van den Broeke, Angela von Deschwanden, César Deschamps-Berger, Brice Van Liefferinge, Stein Tronstad, Yngve Melvær, Quantarctica, an integrated mapping environment for Antarctica, the Southern Ocean, and sub-Antarctic islands. Environmental Modelling and Software, 140, 1-14, 2021.

### Foraminiferal faunal changes in the Shirase Submarine Valley, Lützow-Holm Bay, East Antarctica

Hiroki Matsui<sup>1</sup>, Neneka Takagi<sup>1</sup>, Shiro Hasegawa<sup>2</sup>, Takuya Itaki<sup>3</sup>, and Yusuke Suganuma<sup>4</sup>

<sup>1</sup>Akita University, Akita, Japan

<sup>2</sup>Tohoku University, Sendai, Japan

<sup>3</sup>Geological Survey of Japan, AIST, Tsukuba, Japan

<sup>4</sup>National Institute of Polar Research, Tachikawa, Japan

The warm Circumpolar Deep Water (CDW) in the Southern Ocean can penetrate onto the continental shelf, which leads to increased melting and retreat of the Antarctic ice sheet (Holland et al., 2020). Although modern oceanograhipc observations show inflow of CDW into Lützow-Holm Bay, East Antarctica (Hirano et al., 2020), past changes in CDW intrusion into the bay have not been clearly understood. Here we study foraminifera assemblage from a sediment core LH1a-LGC (46°58.87'S, 38°14.9'E, 797 m water depth) located in Shirase Submarine Valley in Lützow-Holm Bay, to infer potential influence of past CDW. The core length is 119 cm and its lithology is grayish olive sandy silt, collected during the 61st Japanese Antarctic Research Expedition (JARE) (Itaki et al., 2024).

A total of 64 samples larger than 125 μm were observed, and 36 samples of them yielded foraminifera. Planktic foraminifera was intermittently found from the core bottom to ~100 cm, and consistently occurred during ~56–36 cm and for the upper ~6 cm of the core. Similarly, calcareous benthic foraminifera was consistently identified during ~56–36 cm and for the upper ~7 cm of the core, in addition to the sporadic occurrences during ~102–87 cm. In contrast, the occurrences of aggultinated benthic foraminifera was limited to the upper ~15 cm of the core. For calcareous benthic foraminifera, *Globocassidulina biora* (Crespin) was consistently found during ~102–87 cm and ~56–36 cm, whereas *Bulimina aculeata* d'Orbigny dominated for the upper ~7 cm of the core. In Lützow-Holm Bay, *G. biora* is abundant in the Holocene elevated marine deposits where the modern CDW inflow terminates, and *B. aculeata* is a indicator of CDW incursion (Igarashi et al., 2001). In addition, the former species' occurrence is interpreted as a sub-ice shelf environment and the latter species' dominance is associated with an open-marine environment in Marguerite Trough, Antarctic Peninsula (Kilfeather et al., 2011). Thus, the occurences of either *G. biora* or *B. aculeata* in the core LH1a-LGC imply past intrusion of CDW, and the faunal changes through the core can be explained by grounding-line retreat in Lützow-Holm Bay.

### References

Hirano D, Tamura T, Kusahara K, Ohshima KI, Nicholls KW, Ushio S, et al., Strong ice-ocean interaction beneath Shirase Glacier Tongue in East Antarctica. Nature Communications, 11(1), 4221, 2020.

Holland DM, Nicholls KW, Basinski A, The Southern Ocean and its interaction with the Antarctic Ice Sheet. Science, 367(6484), 1326–1330, 2020.

Igarashi A, Numanami H, Tsuchiya Y, Fukuchi M, Bathymetric distribution of fossil foraminifera within marine sediment cores from the eastern part of Lützow-Holm Bay, East Antarctica, and its paleoceanographic implications. Marine Micropaleontology, 42, 125–162, 2001.

Itaki T, Tokuda Y, Ishiwa T, Sasaki S, Suganuma Y, Aoki S, Sedimentological survey by the icebreaker Shirase during JARE-61, Nankyoku Shiryô (Antarctic Record), 68, 21–35, 2024. (in Japanese with English abstract) Kilfeather AA, Cofaigh CÓ, Lloyd JM, Dowdeswell JA, Xu S, Moreton SG, Ice-stream retreat and ice-shelf history in Marguerite Trough, Antarctic Peninsula: Sedimentological and foraminiferal signatures. GSA Bulletin, 123(5–6), 997–1015, 2011.

### Few-shot Learning for High Resolution Velocity Model Estimation of Arctic Subsea Permafrost

<u>Seoje Jeong<sup>1</sup></u> Seung-Goo Kang<sup>2</sup> and Wookeen Chung<sup>1</sup>

1National Korea Maritime & Ocean University

2Korea Polar Research Institute

Subsea permafrost refers to frozen ground that exists beneath the seabed, typically in shallow continental shelves of the Arctic Ocean. It is characterized by high P-wave velocities and poses significant geotechnical and climatic implications in polar regions (Buddo et al., 2022). However, seismic imaging of subsea permafrost is challenging due to strong impedance contrasts between frozen and unfrozen sediments, hindering clear delineation of its base and internal structures (Ramachandran et al., 2011; Kang et al., 2021). Although well-logging data provide accurate in-situ measurements of subsurface properties, their availability in Arctic regions is limited, constraining velocity model estimation and interpretation.

Recent advances in machine learning have been explored to enhance conventional inversion techniques for permafrost velocity imaging. Deep learning methods using convolutional neural networks (CNNs) and encoder-decoder architectures have shown promise in extracting subsurface features from seismic data while minimizing manual intervention (Bustamante et al., 2024; Lee et al., 2022). However, their effectiveness is limited in Arctic seismic survey due to the scarcity of well-logging data required for supervised learning. To overcome this challenge, this study proposes a few-shot learning framework that leverages a small number of well-logging data to estimate high-resolution velocity models. Unlike previous one-shot approaches relying on a single log, the proposed method incorporates multiple borehole data points to enhance structural continuity and reduce overfitting (Fei-Fei et al., 2006; Chen et al., 2022).

While full waveform inversion (FWI) typically reconstructs velocity models by sequentially incorporating low- to high-frequency components of seismic data (Tarantola, 1984), high-frequency FWI in permafrost environments incurs substantial computational cost due to strong velocity contrasts and geological complexity. To mitigate this, reflectivity sections are generated from inversion results and the initial velocity model. These reflectivity images and inversion-derived features serve as inputs to a few-shot learning network, trained with multiple well-log velocity profiles as labels. The network is implemented using a U-Net-based encoder-decoder architecture, optimized for extracting local velocity features from limited training data.

Synthetic training data were generated Arctic subsea permafrost model, which simulates geological conditions representative of the Beaufort Sea. The trained network was then applied to field seismic data from the same region. Despite the limited resolution of the raw seismic data, the model accurately reconstructed key subsurface features, including the geometry and continuity of the permafrost base. The results demonstrate that the proposed few-shot learning approach can produce high-resolution velocity models while significantly reducing computational overhead. This strategy shows strong potential for practical deployment in Arctic environments, where data availability and acquisition logistics are severely constrained.

#### Acknowledgments

This research was supported by Korea Institute of Marine Science & Technology Promotion (KIMST) funded by the Ministry of Oceans and Fisheries, Korea (RS-2023-00259633).

#### References

Buddo I, Misyurkeeva N, Shelokhov I, Chuvilin E, Chernikh A, and Smirnov A, Imaging Arctic permafrost: Modeling for choice of geophysical methods. Geosciences, 12(10), 389, 2022.

Bustamante J, Fabien-Ouellet G, Duchesne MJ, and Ibrahim A, Deep-learning viscoelastic seismic inversion for mapping subsea permafrost. Geophysics, 89(4), R339–R353, 2024.

Chen T, Wang Y, Cai H, Yu G, and Hu G, High resolution pre-stack seismic inversion using few-shot learning. Artificial Intelligence in Geosciences, 3, 203–208, 2022.

Kang SG, Jin YK, Jang U, Duchesne MJ, Shin C, Kim S, Riedel M, Dallimore SR, Paull CK, Choi Y, and Hong JK, Imaging the P-wave velocity structure of Arctic subsea permafrost using Laplace-domain full-waveform inversion. Journal of Geophysical Research: Earth Surface, 126(3), e2020JF005941, 2021.

Lee D, Jeong S, and Chung W, One-shot learning for seismic velocity estimation from well-logging data. SEG Conference Paper, 2024.

Fei-Fei L, Fergus R, and Perona P, One-shot learning of object categories. IEEE Transactions on Pattern Analysis and Machine Intelligence, 28(4), 594–611, 2006.

Ramachandran K, Bellefleur G, Brent T, Riedel M, and Dallimore, S, Imaging permafrost velocity structure using high resolution 3D seismic tomography. Geophysics, 76(5), B187–B198, 2011.

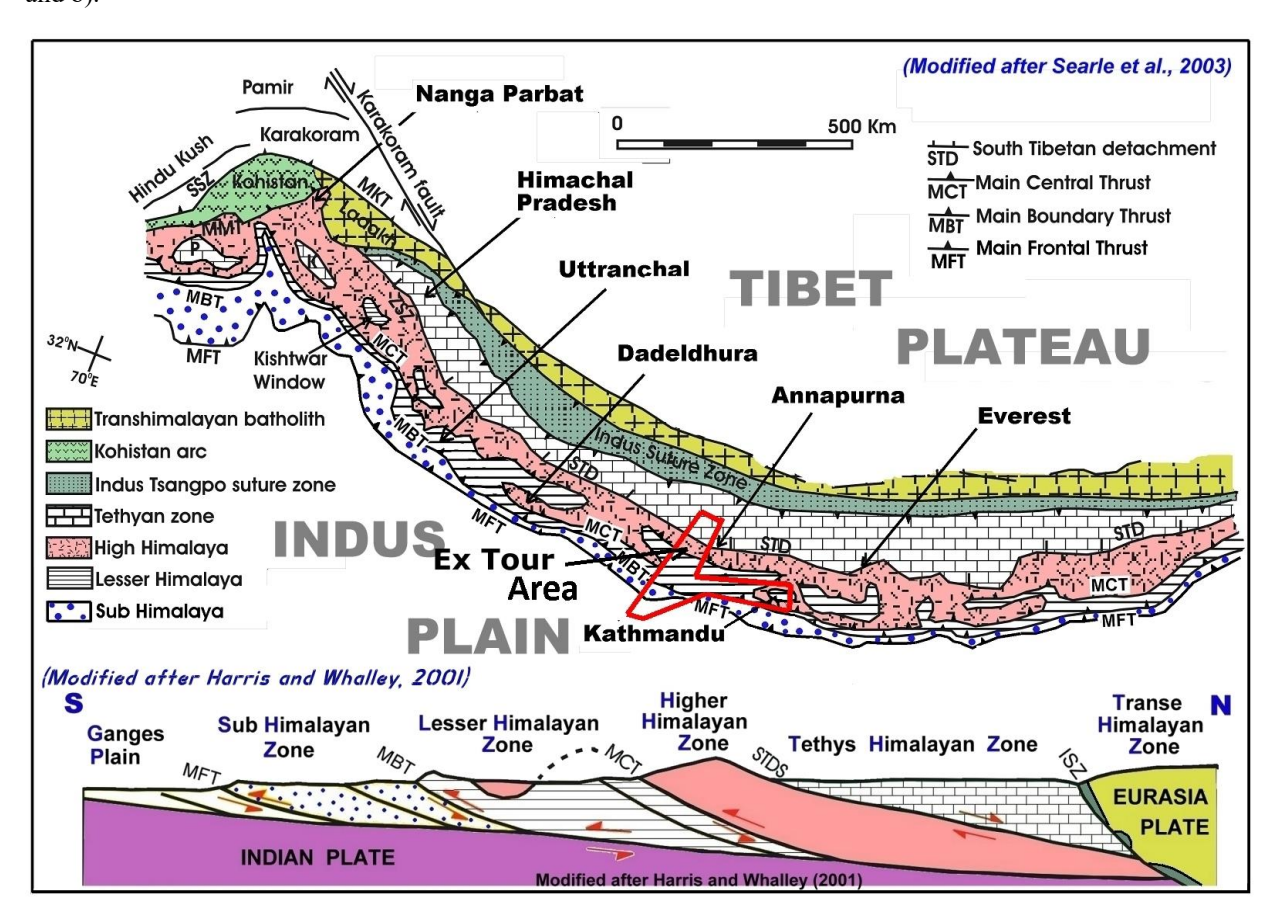
Tarantola A, Inversion of seismic reflection data in the acoustic approximation. Geophysucs, 49(8), 1259-1266, 1983.

### Highlights of the Student Himalayan Field Exercise Tour 13 years

Masaru Yoshida<sup>1</sup> and the Student Himalayan Field Exercise Project<sup>2</sup>

- <sup>1</sup> Gondwana Institute for Geology and Environment and Tri-Chandra Campus, Trivhuvan University (Emeritus Professor)
- <sup>2</sup> co Department of Geosciences, Shimane University. Convenors: Sakai, to (Representative), Yoshida, M. (Co-representative), K. Arita and B.N. Upreti

The Student Himalayan Field Exercise Tour (SHET) has been conducted 13 years since 2012. The Kaligandaki river flowing south between the Annapurna (8091m) and Dhaulagiri (8167m) peaks is the world deepest valley. The exercise tour follows this valley from the north to the south, atarting from the world holly place of Hinduism, Muktinath, and reaching at Pokhara, the famous Himalayan sight seeing city. From Pokhara, the tour goes further southward along some valleys and lastly arrives at the world holliest place of Budhism, Lumbini, in the Gangetic plain. This course is the world best geotour route disclosing all geologic zone of the Himalayan Orogen. Participants of the tour can observe the Tethys Himalayan, Higher Himalayan, Lesser Himalayan, Sub-Himalayan, and Gangetic Alluvial zones from the north to the south, all four major faults dividing the five geologic zones, not only geology but also topography and natural hazards that changes their characteristics in accordance with changing geologic zones. Details of the tour are given in published report books of tours of every year (e.g., Yoshida, 2025a and b).



Geologic outline and cross section of the Himalaya with tor area (red frame)

Participants of 13 years of the tour included 185 students from universities of Japan, Nepal, India, China and Malaysia, 2 high school students from Japan and 23 citizens of Japan and Nepal. Average cost of the tour for a student for 13 years was 204,822 JPY. Support for a student by donations etc. was 31,418 JPY in average of 13 years, which reduced the participation fee for a student to 173,327 JPY. The SHET met no accident and not grave health problem of participants for all 13 years. The evaluation of the tour by participants has been excellent, not only of the great beauty of geology and topography of the Himalaya but also their experience of English-speaking and international environments through out the tour that prompted them to become familiar to those environments (Yoshida, 2016). The presentation will disclose highlight of geology and topography that the tour met through its 13 years experiences.

The 14th SHET is planned to be conducted next March (Yoshida, 2025c), and a crowd funding "Let's help students to study in

the Himalaya!" to help students participating in the SHET-14 has already started (Yoshida, 2025d, in Japanese). Those who are interested in geosciences of polar regions are expected to join tour or crowd funding.

#### References cited

- Yoshida, M., 2016, Student Himalayan Field Exercise Program V--Evaluation of the SHET by participants. Chigaku kyoiku to kagaku undo (Education of geosciences and movement on science), 77, 80-87: http://www.gondwanainst.org/geotours/shet-chidanken-V.pdf.
- Yoshida, M., 2025a, Traversing the Himalayan Orogen 2025: A record of the Student Himalayan Field Exercise Tour in March 2025. Field Science Publishers, Hashimoto, 294 pages: http://www.gondwanainst.org/geotours/2025tour/THO2025-forweb0506.pdf.
- Yoshida,, M., 2025b, Details of the Student Himalayan Field Exercise Program: <a href="http://www.gondwanainst.org/geotours/Studentfieldex\_index.htm">http://www.gondwanainst.org/geotours/Studentfieldex\_index.htm</a> & thtp://www.gondwanainst.org/geotours/shet-chidanken-I-V.pdf .
- Yoshida, M., 2025c, Recruit for the Student Himalayan Field Exercise Tour in 2026: http://www.gondwanainst.org/geotours/2026tour/SHET-14-AdvEN-yoko20250515.pdf
- Yoshida, M., 2025d, Let's student to study the Himalayan geology: http://www.gondwanainst.org/shet-cf.htm